

Revision 1

An Updated Calibration of the Plagioclase-Liquid Hygrometer-Thermometer Applicable to Basalts through Rhyolites

Laura E. Waters^{1*} and Rebecca A. Lange¹

¹Department of Earth and Environmental Sciences
University of Michigan, Ann Arbor, MI 48109 USA

*E-mail: lewaters@umich.edu

Phone: +1-734-764-7421

Fax: +1-734-763-4690

Submitted to: American Mineralogist

October 2014

20

Abstract

21

An updated and expanded data set that consists of 214 plagioclase-liquid equilibrium

22

pairs from 40 experimental studies in the literature is used to recalibrate the thermodynamic

23

model for the plagioclase-liquid hygrometer of Lange et al. (2009); the updated model is

24

applicable to metaluminous and alkaline magmas. The model is based on the crystal-liquid

25

exchange reaction between the anorthite ($\text{CaAl}_2\text{Si}_2\text{O}_8$) and albite ($\text{NaAlSi}_3\text{O}_8$) components, and

26

all available volumetric and calorimetric data for the pure end-member components are used in

27

the revised model. The activities of the crystalline plagioclase components are taken from

28

Holland and Powell (1992). Of the 214 experiments, 107 are hydrous and 107 are anhydrous.

29

Four criteria were applied for inclusion of experiments in the final data set: (1) crystallinities

30

<30%; (2) pure- H_2O fluid saturated; (3) compositional totals (including H_2O component) of 97–

31

101% for hydrous quenched glasses and 98.5-101 for anhydrous quenched glasses; and (4) melt

32

viscosities $\leq 5.2 \log_{10} \text{ Pa s}$. The final data set spans a wide range in liquid composition (45-80

33

wt% SiO_2 ; 1-10 wt% $\text{Na}_2\text{O}+\text{K}_2\text{O}$), plagioclase composition ($\text{An}_{17}-\text{An}_{95}$), temperature (750-

34

1244°C), pressure (0-350 MPa), and H_2O content (0-8.3 wt%). The water solubility model of

35

Zhang et al. (2007) was applied to all hydrous experiments. The standard error estimate on the

36

hygrometer model is 0.35 wt% H_2O , and all liquid compositions are fitted equally well.

37

Application of the model as a thermometer recovers temperatures to within ± 12 degrees, on

38

average. Tests of the hygrometer on anhydrous piston-cylinder experiments in the literature, not

39

included in the regression, show that the model is accurate at all pressures where plagioclase is

40

stable. Applications of the hygrometer are made to natural rhyolites (Bishop Tuff, Katmai and

41

Toba Tuff) with reported H_2O analyses in quartz-hosted melt inclusions from the literature; the

42

results show agreement. Applications of the hygrometer/thermometer are additionally made to

43 natural rhyolites from Iceland and Glass Mountain, CA. The updated model can be downloaded
44 either as a program in Excel format or as a MatLab script from the Data Repository.

45 **Keywords**

46 NEW TECHNIQUE: plagioclase-liquid hygrometer, IGNEOUS PETROLOGY: hygrometer,
47 thermometer, THERMODYNAMICS, PHASE EQUILIBRIA: plagioclase, liquid

48
49

Introduction

50 The composition of plagioclase in magmatic liquids is strongly sensitive to temperature
51 and dissolved water concentrations, and therefore plagioclase has the potential to be used as
52 either a hygrometer or thermometer in volcanic rocks (e.g., Kudo and Weill 1970; Mathez 1973;
53 Glazner 1984; Marsh et al. 1990; Housh and Luhr 1991, Sisson and Grove 1993;
54 Panjasawatwong et al. 1995; Danyushevksy et al. 1997; Putirka 2005, 2008). Recently, Lange et
55 al. (2009) developed a thermodynamic model for the plagioclase-liquid exchange reaction
56 involving the anorthite ($\text{CaAl}_2\text{Si}_2\text{O}_8$) and albite ($\text{NaAlSi}_3\text{O}_8$) components, in which all published
57 calorimetric and volumetric data on the standard state reaction were incorporated into the model
58 in order to independently constrain the effects of temperature and pressure. This allowed
59 available phase-equilibrium experiments in the literature to constrain the effect of melt
60 composition, including dissolved water, on the exchange reaction, thus permitting a plagioclase-
61 liquid hygrometer to be developed.

62 Application of the Lange et al. (2009) model is restricted to plagioclase more calcic than
63 An_{35} and therefore cannot be applied to most rhyolites, owing to the compositional limitation of
64 the experimental data set upon which that model was calibrated. The 2009 hygrometer was
65 calibrated on 71 plagioclase-liquid experiments, of which 45 were hydrous and 26 anhydrous.
66 Three filters were applied to that phase-equilibrium data set: (1) crystallinities < 30%; (2) pure

67 H₂O-fluid saturated; and (3) compositional totals (including H₂O component) of 97-101 % for
68 hydrous quenched glasses. In the 2009 calibration, all melt water concentrations were obtained
69 using the water solubility model of Moore et al. (1998). Experiments were included in the
70 calibration if the analyzed anhydrous oxide components in the glass and the H₂O concentration
71 determined by Moore et al. (1998) summed to values between 97 and 101%.

72 Results from the Couch et al. (2003) study on a low-silica rhyolite were included in the
73 calibration, but owing to the application of the three filters, experiments from other studies on
74 silica-rich liquids with more sodic plagioclases (<An₃₅) were not included. In some cases,
75 experiments were not included because information on modes or glass totals were not published,
76 but otherwise would have passed all three filters (e.g, Larsen, 2006).

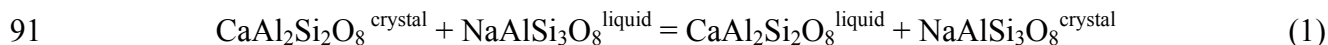
77 Since 2009, there have been several published water-saturated phase-equilibrium
78 experiments on rhyolite, rhyodacite and trachyte liquids that pass all filters (e.g., Martel, 2012;
79 Rader and Larsen, 2013; Martel et al., 2013; Castro et al., 2013; Waters et al., 2014), as well as
80 on basalts (e.g., Parman et al., 2011). Therefore, there is an opportunity to significantly expand
81 the data set upon which the plagioclase-liquid hygrometer/thermometer is calibrated, and to
82 extend its application to a wider range of plagioclase and melt composition, including both
83 rhyolites and alkaline magmas in equilibrium with sodic plagioclase. In addition, the Zhang et
84 al. (2007) water solubility model is used in this study, which is calibrated on the same data set
85 used by Moore et al. (1998) as well as additional data published in the intervening years.

86

87 **Thermodynamic Model of Plagioclase-Liquid Equilibrium**

88 Following Lange et al., (2009), the plagioclase-liquid hygrometer/thermometer is based
89 on the equilibrium exchange reaction of the anorthite (CaAl₂Si₂O₈) and albite (NaAlSi₃O₈)

90 components between crystalline plagioclase and magmatic liquid:



92 At equilibrium:

$$93 \quad \Delta G(T, X, P) = 0 = \Delta H^\circ(T) - T\Delta S^\circ(T) + RT\ln K + \int_0^P \Delta V^\circ_T(P)dP, \quad (2)$$

94 where $\Delta H^\circ(T)$ and $\Delta S^\circ(T)$ are the standard state change in molar enthalpy and entropy,

95 respectively, for the pure crystalline and liquid components, K is the equilibrium constant that

96 accounts for differences in ΔG due to composition, and $\Delta V^\circ_T(P)$ is the change in molar volume

97 for the reaction at temperature T , as a function of pressure, where initial pressure is one bar or

98 0.0001 GPa (shown as 0 in Eq. 2).

99

100 **Standard State Thermodynamic Data**

101 The standard state thermodynamic data used in Equation 2 are listed in Table 1. As

102 stated in Lange et al. (2009), $\Delta H^\circ(T)$, $\Delta S^\circ(T)$ and $\Delta V^\circ_T(P)$ are equivalent to the difference

103 between the enthalpy, entropy and volume of fusion of pure anorthite (An) and pure albite (Ab),

104 respectively (see Eq. 3-5 in Lange et al. 2009). The enthalpy and entropy of fusion for anorthite

105 and albite vary with temperature as follows (where f refers to fusion):

$$106 \quad \Delta H_f(T) = \Delta H_f(T_f) + \int_{T_f}^T [C_P^{\text{liq}}(T) - C_P^{\text{xtl}}(T)] dT \quad (3)$$

$$107 \quad \Delta S_f(T) = \Delta S_f(T_f) + \int_{T_f}^T \left[\frac{C_P^{\text{liq}}(T) - C_P^{\text{xtl}}(T)}{T} \right] dT \quad (4)$$

108 In this study, the heat capacity equations of Berman (1988) are used for crystalline anorthite and
109 albite in Equations 3 and 4 (Table 1). Tenner et al. (2007) used the drop calorimetric

110 measurements of Stebbins et al. (1983) and Richet and Bottinga (1984a), together with the heat

111 capacity equations of Berman (1988) and Richet (1987) for albite crystal and glass, respectively,

112 to derive internally consistent values for the enthalpy of fusion for albite at its 1-bar fusion

113 temperature and the heat capacity of liquid $\text{NaAlSi}_3\text{O}_8$ (Table 1). A similar exercise is followed
114 in this study to derive internally consistent values for the 1-bar enthalpy of fusion for anorthite
115 and the heat capacity of liquid $\text{CaAl}_2\text{Si}_2\text{O}_8$ from the drop calorimetric data of Stebbins et al.
116 (1983) and Richet and Bottinga (1984b). The details of this exercise are provided in Appendix
117 A, and the results are given in Table 1.

118 Calculation of $\Delta V^\circ_T(P)$ in Equation 2 requires information on the molar volume, thermal
119 expansion, and compressibility for both liquid and crystalline anorthite and albite (Table 1). The
120 data and equations used in this study are identical to those used in Lange et al. (2009), where a
121 detailed discussion of the volumetric terms is provided. We note, however, that there was a
122 decimal point error in Table 1 of Lange et al. (2009) for the $\delta V/\delta P$ values for albite and anorthite
123 liquid, respectively, which are correct in Table 1 of this study.

124

125 **Activity-Composition Relations**

126 The natural log of the equilibrium constant in Equation 2 is equal to:

$$127 \quad \ln(K) = \ln\left(\frac{a_{\text{CaAl}_2\text{Si}_2\text{O}_8}^{\text{liquid}}}{a_{\text{NaAlSi}_3\text{O}_8}^{\text{liquid}}}\right) + \ln\left(\frac{a_{\text{NaAlSi}_3\text{O}_8}^{\text{crystal}}}{a_{\text{CaAl}_2\text{Si}_2\text{O}_8}^{\text{crystal}}}\right). \quad (5)$$

128 The activity terms in Equation 5 are further broken down to the mole fractions (X) and activity
129 coefficients (γ) for the crystalline and liquid components in Equations 6a and 6b, respectively:

$$130 \quad \ln\left(\frac{a_{\text{NaAlSi}_3\text{O}_8}^{\text{crystal}}}{a_{\text{CaAl}_2\text{Si}_2\text{O}_8}^{\text{crystal}}}\right) = \ln\left(\frac{\gamma_{\text{NaAlSi}_3\text{O}_8}^{\text{crystal}}}{\gamma_{\text{CaAl}_2\text{Si}_2\text{O}_8}^{\text{crystal}}}\right) + \ln\left(\frac{X_{\text{NaAlSi}_3\text{O}_8}^{\text{crystal}}}{X_{\text{CaAl}_2\text{Si}_2\text{O}_8}^{\text{crystal}}}\right) \quad (6a)$$

$$131 \quad \ln\left(\frac{a_{\text{CaAl}_2\text{Si}_2\text{O}_8}^{\text{liquid}}}{a_{\text{NaAlSi}_3\text{O}_8}^{\text{liquid}}}\right) = \ln\left(\frac{\gamma_{\text{CaAl}_2\text{Si}_2\text{O}_8}^{\text{liquid}}}{\gamma_{\text{NaAlSi}_3\text{O}_8}^{\text{liquid}}}\right) + \ln\left(\frac{X_{\text{CaAl}_2\text{Si}_2\text{O}_8}^{\text{liquid}}}{X_{\text{NaAlSi}_3\text{O}_8}^{\text{liquid}}}\right). \quad (6b)$$

132 The mole fraction of anorthite and albite in the plagioclase crystal is based on the abundance of
133 Ca and Na in the A site alone and is determined from microprobe analyses. In both the
134 hygrometer of Lange et al. (2009) and the updated hygrometer in this study, the activity

135 coefficient (γ) terms for the crystalline components are obtained from the THERMOCALC
136 program (<http://www.earthscii.unimelb.edu.au/tpg/thermocalc/>), which is based on the Holland
137 and Powell (1992) model for plagioclase. In this study, the activity coefficient terms for
138 crystalline plagioclase have been parameterized for a range of compositions (0 to 100 mol% An)
139 and a range of temperatures (600 to 1350°C); the details of the parameterization are given in
140 Appendix B.

141 The activity-composition relations for the liquid components (Equation 6b), forms the
142 basis of the hygrometer of both Lange et al. (2009) and this study. The mole fractions of the
143 *liquid* anorthite and albite components are defined following Carmichael (1977):

$$144 \quad X_{\text{CaAl}_2\text{Si}_2\text{O}_8}^{\text{ideal liquid}} = 64.0 \left(X_{\text{CaO}}^{\text{liq}} \right) \left(X_{\text{Al}_2\text{O}_3}^{\text{liq}} \right) \left(X_{\text{SiO}_2}^{\text{liq}} \right)^2 \quad (7a)$$

$$145 \quad X_{\text{NaAlSi}_3\text{O}_8}^{\text{ideal liquid}} = 18.963 \left(X_{\text{Na}_2\text{O}}^{\text{liq}} \right)^{0.5} \left(X_{\text{Al}_2\text{O}_3}^{\text{liq}} \right)^{0.5} \left(X_{\text{SiO}_2}^{\text{liq}} \right)^3 \quad (7b)$$

146 The coefficients in Equations 7a and 7b ensure that the mole fraction of pure anorthite and pure
147 albite liquid, respectively, each take the value of one. The ratio of the activity coefficient terms
148 (γ) in Equation 6b is modeled as a linear function of liquid composition, including the dissolved
149 H₂O component:

$$150 \quad \ln \left(\frac{\gamma_{\text{CaAl}_2\text{Si}_2\text{O}_8}^{\text{liquid}}}{\gamma_{\text{NaAlSi}_3\text{O}_8}^{\text{liquid}}} \right) = a + \frac{b}{T} + \sum d_i X_i + d_{\text{H}_2\text{O}} X_{\text{H}_2\text{O}} \quad (8)$$

151 The terms a , b and d_i are parameters to be fitted from the calibration of plagioclase-liquid
152 equilibrium experiments, $X_{\text{H}_2\text{O}}$ is the mole fraction of dissolved H₂O in the melt, and X_i the mole
153 fraction of other oxide components (e.g., SiO₂, Al₂O₃, etc.), where “ i ” is defined as $i=1$ to n ,
154 where n is the number of oxide components in Equation 8. A temperature term (b/T) is added to
155 account for the dependence of H₂O speciation (e.g., OH⁻ groups and molecular H₂O) on
156 temperature, which is discussed extensively in Lange et al. (2009).

157

158 Calibration Equation

159 Because the goal is to calibrate a plagioclase-liquid hygrometer, a regression equation is
160 developed with $X_{\text{H}_2\text{O}}$ as the dependent variable on the left side of the equation. To accomplish
161 this, first the equilibrium reaction is shown in Equation 9, where x (defined in Equation 10)
162 includes all of the standard-state thermodynamic data, crystalline activity terms, and the ideal
163 contributions to the liquid anorthite and albite activities.

$$164 \quad 0 = x + a + \frac{b}{T} + \sum X_i d_i + X_{\text{H}_2\text{O}}(d_{\text{H}_2\text{O}}) \quad (9)$$

165 where

$$166 \quad x = \frac{\Delta H^\circ(T)}{RT} - \frac{\Delta S^\circ(T)}{R} + \frac{\int_1^P \Delta V_T^\circ(P) dP}{RT} + \ln \left(\frac{X_{\text{CaAl}_2\text{Si}_2\text{O}_8}^{\text{ideal liquid}}}{X_{\text{NaAlSi}_3\text{O}_8}^{\text{ideal liquid}}} \right) + \ln \left(\frac{a_{\text{NaAlSi}_3\text{O}_8}^{\text{crystal}}}{a_{\text{CaAl}_2\text{Si}_2\text{O}_8}^{\text{crystal}}} \right) \quad (10)$$

167 Equation 9 is then rearranged so that $X_{\text{H}_2\text{O}}$ is the dependent variable in Equation 11.

$$168 \quad X_{\text{H}_2\text{O}}(-d_{\text{H}_2\text{O}}) = x + a + \frac{b}{T} + \sum X_i d_i \quad (11)$$

169 Both sides of Equation 11 are divided through by $-d_{\text{H}_2\text{O}}$, which leads to:

$$170 \quad X_{\text{H}_2\text{O}} = mx + a' + \frac{b'}{T} + \sum X_i d_i' \quad (12)$$

171 where

$$172 \quad m = -\frac{1}{d_{\text{H}_2\text{O}}}, \quad a' = \frac{a}{-d_{\text{H}_2\text{O}}}, \quad b' = \frac{b}{-d_{\text{H}_2\text{O}}}, \quad d_i' = \frac{d_i}{-d_{\text{H}_2\text{O}}} \quad (13)$$

173 Lange et al. (2009) found that the most advantageous form of the regression equation was made
174 by substituting wt% H₂O for $X_{\text{H}_2\text{O}}$, which allows for the calculation of wt% H₂O without having
175 prior information about the concentration of dissolved melt H₂O. This empirical change does not
176 diminish the quality of the final calibration. Thus, the final form of the regression equation is:

$$177 \quad \text{wt\% H}_2\text{O} = m'x + a'' + \frac{b''}{T} + \sum X_i d_i'' \quad (14)$$

178

179 Plagioclase-Liquid Phase Equilibrium Data

180 In order to perform a regression on Equation 14, plagioclase-liquid equilibrium
181 experiments from the literature are required. A final data set of 214 plagioclase-liquid
182 equilibrium pairs (107 hydrous; 107 anhydrous) was chosen from an initially larger set of
183 experiments, after application of the following four filters: (1) pure-H₂O fluid saturated; (2)
184 compositional totals (including H₂O component) of 97–101% for hydrous quenched glasses and
185 98.5-101 for anhydrous quenched glasses; (3) crystallinities $\leq 30\%$; and (4) melt viscosities ≤ 5.2
186 \log_{10} Pa s. The purpose of these filters is to exclude experiments where analytical uncertainties
187 may be too high and/or where equilibrium may not have been attained. Lange et al. (2009)
188 provide a detailed explanation of the first three filters. The last filter is new to this study
189 (although it applies to the data set used in Lange et al. 2009) and it is another mechanism to
190 exclude experiments where equilibrium may not have been obtained owing to slow diffusion in
191 the melt phase. The four filters were applied uniformly to experiments from the literature, and
192 although some experiments may have been excluded that achieved equilibrium and/or had small
193 analytical uncertainties, the uniform application of all four filters prevented several
194 disequilibrium experiments and/or those with low analytical totals from being included in an
195 unbiased manner. In this study, the H₂O solubility model of Zhang et al. (2007) is used to
196 calculate the water concentration in all experimental liquids; the model has a 1σ error of 0.34
197 wt% H₂O.

198 The final data set of 214 plagioclase-liquid equilibrium experiments is obtained from 40
199 studies (Aigner-Torres et al., 2007; Bartels et al., 1991; Berndt et al., 2005; Blatter and
200 Carmichael, 2001; Blundy, 1997; Botcharnikov et al., 2008; Brugger et al., 2003; Castro et al.,
201 2013; Couch et al., 2003; Costa et al., 2004; Gardner et al., 1995; Grove et al., 1982, 1997, 2003;
202 Grove and Bryan, 1983; Grove and Juster, 1989; Holtz et al., 2005; Juster et al., 1989; Larsen,

203 2006; Luhr, 1990; Mahood and Baker, 1986; Martel et al., 1999, 2013; Martel, 2012; Moore and
204 Carmichael, 1998; Parman et al., 2011; Rader and Larsen, 2013; Sack et al., 1987; Sisson et al.
205 (1993a,b); Snyder et al., 1993; Takagi et al., 2005; Thy et al., 2006; Toplis et al., 1994; Toplis
206 and Carroll, 1995; Tormey et al., 1987; Wagner et al., 1995; Waters et al., (in review); Vander
207 Auwera et al., 1998; Yang et al., 1996) and greatly expands the compositional range relative to
208 the data set used by Lange et al. (2009). The final hydrous data set (Appendix C) spans a wide
209 range of liquid composition (45-80 wt% SiO₂), plagioclase composition (An₁₇₋₉₅), temperature
210 (750-1125°C), pressure (48-350 MPa), and water concentration (1.4-8.3 wt%), which is
211 illustrated in Fig 1A and 1B. The anhydrous data set (Appendix C) is dominated by basaltic melt
212 compositions, but extends to 70 wt% SiO₂ (Brugger et al., 2003), which marks the limit of the
213 melt viscosity filter. The plagioclase compositions in anhydrous melts are also more restricted
214 (An₅₁₋₉₀), as well as the temperature range (1072-1244°C). The 214 experiments include several
215 alkaline liquids (as defined by Irvine and Baragar, 1971; Fig. 2) in equilibrium with plagioclase
216 from the studies of Sack et al. (1987), Luhr (1990), Martel et al. (2013), and Waters et al. (in
217 review).

218 Another illustration of the compositional range of the calibration data set is seen in a plot
219 of plagioclase composition (mol% An) vs. the An-number of the equilibrium melt composition
220 (Fig. 3). An-number is defined as $X_{CaAl_2Si_2O_8}^{liquid} / (X_{NaAlSi_3O_8}^{liquid} + X_{CaAl_2Si_2O_8}^{liquid})$, using Equations 7a and 7b.

221 Figure 3 shows that for each liquid An-number there is a wide range of plagioclase compositions
222 that can crystallize under equilibrium conditions, depending on other compositional components
223 in the melt, especially dissolved water concentration, as well as temperature and pressure. The
224 effect of dissolved water is clearly seen; plagioclase is systematically more calcic in hydrous vs.
225 anhydrous liquids. What is most striking is the wide range in plagioclase compositions (An₁₇₋₆₀)

226 at melt An-numbers ≤ 20 , and the question is whether a multiple linear regression of Equation 14
227 can adequately model the data in Figure 3. The calibration data set is projected onto the
228 anhydrous and hydrous binary loop phase diagrams to further illustrate the effect of temperature
229 and melt composition on plagioclase composition in the supplemental material (Appendix D).

230

231 **RESULTS**

232 **Hygrometer/Thermometer Regression Results**

233 A series of un-weighted, least squares, multiple linear regressions of Equation 14 were
234 performed using the backward stepwise method. The initial regression included 11 fitted terms
235 (m' , a'' , b'' and d_i'' , where $i = \text{SiO}_2, \text{TiO}_2, \text{Al}_2\text{O}_3, \text{FeO}^{\text{T}}, \text{MgO}, \text{CaO}, \text{Na}_2\text{O}$ and K_2O). The only
236 component that did not pass the t-test was TiO_2 , but all others were statistically significant,
237 leading to 10 fitted terms. However, the magnitude of the fitted K_2O term was anomalously
238 large, and so a new term ($\text{K}_2\text{Al}_2\text{O}_4$) was constructed, where the moles of K_2O in each sample
239 were subtracted from the moles of Al_2O_3 , leading to a revised Al_2O_3^* term. This change
240 improved the regression results, whereas a similar approach to construct a $\text{Na}_2\text{Al}_2\text{O}_4$ term did
241 not. The results of the final regression are shown in Table 2; the fit has an R^2 value of 0.98 and a
242 standard error on the estimate of 0.35 wt% H_2O , which is comparable to the 1σ error of ± 0.34
243 wt% on the H_2O solubility model of Zhang et al. (2007). Therefore the hygrometer recovers the
244 wt% H_2O in each experimental liquid within the uncertainty of its value in the calibration data
245 set. Attempts to reduce the standard error estimate in half, to levels well below the
246 1σ uncertainty in the water contents of the experimental liquids by more than doubling the
247 number of fitted terms (e.g., 26 fitted terms in Zeng et al., 2014), should be viewed with caution
248 as this can lead to an over fit to the experimental data set. A plot of measured vs. calculated H_2O
249 concentrations is shown in Figure 4A, along with a histogram of residuals in Figures 4B. The

250 residuals plotted in Figure 5A-F show that the quality of the fit is equally good for all melt
251 compositions (wt% SiO₂, wt% Na₂O+K₂O, An-number), as well as plagioclase composition,
252 temperature and melt viscosity. Also shown in Figure 5 are the residuals when the model of
253 Lange et al. (2009) is applied. This former model breaks down when the An-number of the
254 liquid is < 15, which is also when SiO₂ concentrations exceed 70 wt% and total alkalis exceed 8
255 wt%.

256 It is also possible to use the plagioclase-liquid model as a thermometer rather than a
257 hygrometer. When melt composition, plagioclase composition, pressure and wt% H₂O are all
258 inputs, temperature can be varied until the calculated wt% H₂O value matches the input wt%
259 H₂O. A plot of measured vs. calculated temperatures is shown in Figure 6A, along with a
260 histogram of residuals in Figures 6B. Figure 7 illustrates that the model (Equation 14; Tables 1
261 and 2) recovers temperatures equally well for all experimental temperatures (750-1244°C) and
262 all melt compositions (45-80 wt% SiO₂). The average difference between the reported and
263 calculated temperature for the 214 experiments is 12 degrees (10 and 14 degrees, respectively,
264 for anhydrous and hydrous experiments). The excellent recovery in temperature is notable
265 because the regression of Equation 14 did not minimize residuals for temperature, but for wt%
266 H₂O. Therefore, the advantage of this thermometer is that it is not based on a separate regression
267 from the hygrometer, but is the exact same model. We attribute the internal consistency to the
268 incorporation of thermodynamic data on the standard-state reaction (Table 1). For comparison,
269 the plagioclase-liquid thermometer presented by Putirka (2008) yields calculated temperatures
270 for our calibration data set that are within 18°C, on average (12 and 23 degrees, respectively, for
271 anhydrous and hydrous experiments), as shown in Figure 7.

272

273 **Tests of the Accuracy of the Hygrometer/Thermometer Model**

274 The newly calibrated plagioclase-liquid hygrometer/thermometer can be tested against
275 several experimental studies not included in the regression. For example, anhydrous piston-
276 cylinder experiments on plagioclase-liquid equilibrium pairs at 1.0-1.2 GPa (Bartels et al., 1991;
277 Draper and Johnston, 1992; Appendix E) allow an examination of how well the volumetric terms
278 in the hygrometer/thermometer model capture the effect of increasing pressure on plagioclase-
279 liquid equilibrium, independent of melt water concentration. The model outputs water
280 concentrations that range from -0.4 to 0.5 wt% for these anhydrous high-pressure experiments,
281 which is well within the range of residuals for the 1-bar anhydrous experiments used in the
282 calibration (see Figure 4B). Therefore, the results demonstrate that the hygrometer can be
283 applied to all pressures where plagioclase is stable.

284 A similar test can be made on hydrous plagioclase-liquid experiments on basalts
285 conducted under H₂O-undersaturated conditions (Hamada and Fujii, 2008) and on rhyolites
286 conducted under mixed H₂O-CO₂ fluid conditions (Almeev et al., 2012), where the quenched
287 glasses in the run products were all analyzed directly for dissolved H₂O concentration using
288 FTIR (Fourier Transform Infrared) spectroscopy (Appendix E). The average difference between
289 analyzed and calculated wt% H₂O is 0.6 and 0.4, respectively, for the basalt and rhyolite
290 experiments (Fig. 8), again indicating good agreement within the combined uncertainties of the
291 hygrometer model (see residuals in Fig. 4) and the experiments (including analyzed water and
292 reported temperature; an uncertainty of five degrees can lead to an uncertainty in calculated
293 water of ± 0.2 wt% H₂O).

294 Another test of the hygrometer, in terms of its ability to be extrapolated to rhyolitic melts
295 (72-77 wt% SiO₂) under anhydrous conditions, is made by applying it those experiments in
296 Brugger et al. (2003) not included in the calibration data set because melt viscosities ranged from

297 5.3 to 6.6 log₁₀ Pa-s (Note that three experiments from that study with lower melt viscosities
298 were included in the regression; Appendix C.) Experiments with high viscosities (>5.3 log₁₀ Pa-
299 s) were excluded from the calibration, as the high viscosities may prevent achievement of
300 equilibrium due to low melt diffusivity. The Brugger et al. (2003) rhyolite experiments were held
301 for seven days and the starting material was 100% glass. The plagioclase compositions that
302 crystallized from these experiments lead to calculated wt% H₂O values that range from -0.3 to +
303 0.3 wt% H₂O (Fig. 9), which is well the within the range of residuals for anhydrous experiments
304 used to calibrate this hygrometer (see Fig. 4). These results suggest that is it is possible to attain
305 equilibrium plagioclase compositions at high melt viscosities if the samples are held long enough
306 and the starting material is glass. The good agreement further indicates that the updated
307 hygrometer model accurately captures the effect of variable melt composition (from basalt to
308 rhyolite) on plagioclase composition, independent of the effects of dissolved water
309 concentration, temperature and pressure.

310

311 **The Effects of Melt composition, Dissolved Water Concentration, Temperature and**

312 **Pressure on Plagioclase Composition**

313 The effect of melt composition, temperature, pressure and dissolved water concentration
314 on the composition of plagioclase is illustrated in Fig. 10. In that diagram, calculated values of
315 wt% H₂O in melt vs. equilibrium plagioclase composition are plotted at constant 100 MPa for
316 three different melt compositions, at temperatures that each is reasonably found in nature. The
317 compositions of the basalt (50.5 wt% SiO₂; 1200°C), andesite (61.8 wt% SiO₂; 1000°C), and
318 rhyolite (75.4 wt% SiO₂; 800°C) used for this figure are given in Table 3. Not surprisingly, for a
319 given plagioclase composition (e.g., An₅₀), the rhyolite at lower temperature requires a higher
320 dissolved water concentration than a basalt at higher temperature, in order to be in equilibrium

321 with the same plagioclase composition. What is also illustrated in Figure 10 is the strong
322 sensitivity of plagioclase composition to dissolved water concentration. An increase of just 0.5
323 wt% dissolved H₂O leads to an increase in the anorthite component of ~20 mol% in the
324 equilibrium plagioclase, with the effect of water strongest at high temperature. Additionally,
325 temperature exerts a strong influence on calculated values of wt% H₂O, as seen in the dashed
326 lines associated with a change of ± 20 degrees in the input temperature for each melt
327 composition (Fig. 10). At relatively low and high temperatures, (800 and 1200 °C), a variation
328 of ± 20 degrees in the input temperature leads to a variation in calculated water of ± 0.5 and ± 0.2
329 wt%, respectively. This result underscores the necessity of evaluating temperature
330 independently and accurately (e.g., through Fe-Ti oxide thermometry) in order to apply the
331 plagioclase-liquid hygrometer.

332 In stark contrast to the effect of temperature, pressure exerts little influence on the
333 plagioclase-liquid hygrometer. This is illustrated in Fig. 11, where the effect of increasing
334 pressure on the calculated wt% H₂O is shown for rhyolite, andesite and basalt melts (at 800,
335 1000, and 1200°C, respectively) for the same plagioclase composition of An₅₀. The results show
336 a weak pressure dependence on the calculated value of wt% H₂O, where an increase from 0 to
337 1.2 GPa leads to a small increase of 0.3 and 0.2 wt% H₂O, at 800 and 1200°C, respectively. The
338 slight temperature dependence on the magnitude of the pressure effect is due to the fact that the
339 volume change for the exchange reaction varies with temperature. Nonetheless, the reason for
340 the nearly negligible effect of pressure on the hygrometer, which contrasts with the very large
341 effect of temperature, is due to the small magnitude of the volume change for the exchange
342 reaction, particularly when compared to the large magnitude of the enthalpy of the exchange
343 reaction, all of which is discussed at length in Lange et al. (2009).

344

345

Discussion

346 **Application of the Hygrometer to Natural Rhyolites with Analyzed Melt Inclusion Water**

347 **Contents**

348 In the following section, the plagioclase-liquid hygrometer is applied to rhyolites from:

349 (1) the Bishop Tuff, California; (2) the Katmai 1912 eruption, Alaska; and (3) the Toba Tuff,

350 Sumatra, Indonesia. The rhyolites from these three localities permit a test of the plagioclase-

351 liquid hygrometer against reported H₂O contents measured in quartz-hosted melt inclusions (MI)

352 from the literature.

353

354 **Bishop Tuff.**

355 The Bishop Tuff is the product of a >600 km³ Plinian eruption of rhyolite magma, which

356 was saturated in nine to twelve mineral phases: quartz + plagioclase + sanidine + biotite +

357 titanomagnetite + ilmenite + apatite + zircon ± allanite ± orthopyroxene ± monazite ± augite ±

358 pyrrhotite. Whole-rock compositions are reported for 14 samples (75.3-77.6 wt% SiO₂) in

359 Hildreth (1977), for which plagioclase (An₁₃-An₂₄), titanomagnetite and ilmenite compositions

360 are also provided. The Fe-Ti oxide analyses from Hildreth (1977) were input into the Ghiorso

361 and Evans (2008) thermometer, leading to pre-eruptive temperatures that range between ~700-

362 810°C. Application of the plagioclase-liquid hygrometer to these samples results in H₂O

363 contents that range from 3.9-6.8 wt% (Fig. 12), with water concentrations increasing

364 systematically with decreasing temperature. Also shown in Fig. 12 are the range of H₂O contents

365 measured in quartz-hosted melt inclusions from Wallace et al. (1999) and Anderson et al. (2000)

366 for the Early (Ig1Eb), Middle (Ig2Ea) and Late (Ig2NWa; Ig2NWb) units of the Bishop Tuff,

367 which are plotted as a function of Fe-Ti oxide temperatures reported for those units by Hildreth

368 and Wilson (2007). The H₂O contents calculated with the plagioclase-liquid hygrometer broadly
369 match the H₂O contents measured in quartz-hosted melt inclusions from the Early, Middle and
370 Late Bishop Tuff (Fig. 12).

371

372 **Katmai 1912 Eruption.**

373 The Katmai 1912 eruption produced 11-15 km³ of magma ranging from 58-75 wt% SiO₂.
374 The rhyolitic end-member is a crystal-poor (0.5-2%), high-silica rhyolite (76.9 wt% SiO₂) that is
375 saturated with up seven mineral phases: quartz + plagioclase + titanomagnetite + ilmenite +
376 hypersthene + pyrrhotite ± amphibole. Analyzed H₂O concentrations in quartz-hosted melt
377 inclusions range from 3.0-5.2 wt% (Lowenstern, 1993) and 4.2-4.7 wt% H₂O (Wallace, 2005).
378 For comparison, application of the plagioclase-liquid hygrometer using whole-rock compositions
379 (76.6-77.4 wt% SiO₂), plagioclase compositions (An₂₅₋₂₉), and pre-eruptive temperatures (805-
380 850°C; recalculated with Ghiorso and Evans, 2008) obtained from Fe-Ti oxide analyses reported
381 in Hildreth (1983) lead to values that range from 3.9-5.0 wt% H₂O. This result shows that the
382 plagioclase-liquid hygrometer is fully consistent with the published melt inclusion analyses
383 reported in Lowenstern (1993) and Wallace (2005).

384 This consistency further suggests that plagioclase and quartz were co-liquidus phases in
385 the Katmai rhyolite. This inference is confirmed by some of the phase-equilibrium experiments
386 reported for Katmai rhyolite in Coombs and Gardner (2001), although at 800-850°C the
387 plagioclase-in and quartz-in curves are both located at P_{H₂O} = 100-40 MPa, which leads to a
388 maximum H₂O concentration in the melt during crystallization of these phases of ≤ 4.1 wt%.
389 This discrepancy of ~1 wt% H₂O between the results from the phase-equilibrium experiments
390 and those from the melt inclusion analyses and the plagioclase-liquid hygrometer may be
391 attributable to the relatively high viscosity of the liquids (>5.5 log₁₀ Pa-s) in the phase-

392 equilibrium experiments at $P_{\text{H}_2\text{O}} \leq 100$ MPa.

393

394 **Toba Tuff.**

395 The youngest unit of the Toba tuff (YTT) is 2,800 km³ (Chesner, 1998) of zoned rhyolite
396 (68-76 wt% SiO₂) (Chesner and Rose, 1991), which is saturated in ten mineral phases: quartz,
397 plagioclase, sanidine, biotite, amphibole, orthopyroxene, titanomagnetite, allanite, zircon, and
398 ilmenite. The compositions of Fe-Ti oxides reported in Chesner (1998) are incorporated into the
399 geothermometer of Ghiorso & Evans (2008) to calculate three pre-eruptive temperatures for the
400 YTT (687, 722, and 732 °C). The plagioclase-liquid hygrometer is applied to pre-eruptive
401 temperatures, the average plagioclase composition found in the YTT (An₃₄) and the bulk
402 composition of the more evolved end member of the YTT (sample #54; Chesner 1998) to
403 calculate melt H₂O contents of 6.6 to 7.9 wt% H₂O (Fig. 13). Using the water solubility model
404 of Zhang et al. (2007), these H₂O contents (6.6-7.9 wt%) correspond to $P_{\text{H}_2\text{O}}(\text{total})$ values
405 ranging from ~230 to 330 MPa for the YTT melt composition. The water contents derived from
406 the plagioclase-liquid hygrometer are compared to the results of phase equilibrium experiments
407 on the Toba Tuff conducted by Gardner et al. (2002) in Figure 13. The water contents obtained
408 by applying the hygrometer to plagioclase from the natural sample match the water contents at the
409 plagioclase-in curve experimentally determined by Gardner et al. (2002), which implies that the
410 plagioclase-hygrometer accurately predicts-pre-eruptive melt H₂O contents for the average of the
411 reported plagioclase compositions.

412 Pre-eruptive melt H₂O and CO₂ contents measured by FTIR in quartz hosted melt
413 inclusions from the Younger Toba Tuff reported by Chesner and Luhr (2010) range from 3.9-6.4
414 wt% and 10-175 ppm, respectively. The plagioclase-liquid hygrometer calculates a maximum
415 melt H₂O content of 7.9 wt% at 687°C, which is ~1.5 wt% higher than the maximum value

416 obtained from melt inclusions (Chesner and Luhr, 2010). The discrepancy between the
417 plagioclase hygrometer and the melt inclusion analyses can be accounted for by the observation
418 that plagioclase crystallizes at higher P_{H_2O} than quartz in this rhyolite composition at any given
419 temperature at upper crustal conditions, according to the experimental phase diagram of Gardner
420 et al. (2002) in Fig. 13. Therefore, the H_2O contents measured in quartz-hosted melt inclusions
421 are not always applicable to the conditions of plagioclase growth, which is seen in liquids
422 (typically those with An-numbers >4) where quartz saturates at a lower P_{H_2O} value lower than
423 that for plagioclase.

424 425 **Application of the hygrometer to rhyolites for which H_2O and/or temperature is unknown**

426 The plagioclase-liquid hygrometer/thermometer provides an opportunity to obtain pre-
427 eruptive intensive variables for samples where data from melt inclusions are not available or
428 where geo-thermometers may not be applied. Here, melt water contents are calculated for lavas
429 from Glass Mountain, Long Valley, CA and Thingmuli Volcano, Iceland, and pre-eruptive
430 temperatures are calculated for rhyolites from the Torfajökull volcanic complex, Iceland.

431 432 **Glass Mountain Rhyolites, Long Valley, CA.**

433 The hygrometer is applied to rhyolites from Glass Mountain, Long Valley, CA to obtain
434 the first estimates of their pre-eruptive water contents. Glass Mountain is composed of high-
435 silica (76.8-77 wt% SiO_2) rhyolite lavas that are saturated in \geq seven mineral phases: plagioclase
436 + sanidine + ilmenite + titanomagnetite + zircon + allanite + apatite \pm biotite (Metz & Mahood,
437 1991). Compositions of coexisting ilmenite and titanomagnetite phenocrysts are reported for
438 eight obsidian lavas in Metz & Mahood (1991) and input into the thermometer of Ghiorso &
439 Evans (2008) to obtain pre-eruptive temperatures that range from 698-725°C. Application of the

440 plagioclase-liquid hygrometer using these temperatures with the plagioclase (An_9 - An_{22}) and
441 liquid compositions reported in Metz & Mahood (1991) results in pre-eruptive water contents
442 that range from 6.6-7.7 wt% H_2O for the Glass Mountain rhyolites. The fact that lower water
443 contents are not recorded by the plagioclase in these degassed obsidian samples, with LOI (loss
444 on ignition) of <0.4 wt% (Metz and Mahood, 1991), suggests that magma ascent was sufficiently
445 rapid that the loss of dissolved water led to a rapid increase in melt viscosity and decrease in
446 chemical diffusivity, similar to the effects of rapid cooling, leading to a termination in
447 plagioclase nucleation and growth, which is experimentally demonstrated in Waters et al. (in
448 review).

449

450 **Icelandic Rhyolites: Thingmuli and Torfajökull Volcanic Complexes.**

451 Thingmuli Volcano in eastern Iceland erupted a suite of lavas that span a range of
452 compositions from tholeiitic basalt to rhyolite (47.1-75.7 wt% SiO_2 ; Carmichael, 1964).
453 Compositions are reported for whole rocks (Carmichael, 1964), as well as for mineral phases,
454 including plagioclase, ilmenite, and titanomagnetite (Carmichael, 1967). Here, we re-calculate
455 temperatures (917 and 865°C, respectively) for two silicic lavas (59 and 70 wt% SiO_2) (#16 and
456 #18; Carmichael, 1964), using the Fe-Ti oxide thermometer of Ghiorso and Evans (2008).
457 Application of the plagioclase-liquid hygrometer to these two samples, which crystallized sparse
458 plagioclase phenocrysts (An_{42} and An_{38} , respectively), leads to melt water concentrations of 3.5
459 and 3.6 wt%, respectively, at the time of phenocryst crystallization.

460 In contrast to the case for Thingmuli silicic lavas, where pre-eruptive temperatures are
461 known from two Fe-Ti oxides, rhyolites from the Torfajökull volcanic complex contain a mineral
462 assemblage that does not permit thermometry to be applied. The Torfajökull rhyolites are

463 saturated with \geq four mineral phases: plagioclase + alkali feldspar + clinopyroxene +
464 titanomagnetite \pm olivine \pm apatite \pm zircon \pm biotite \pm amphibole; neither ilmenite nor
465 orthopyroxene is found (MacDonald et al., 1990). Although pre-eruptive temperatures are not
466 known for these rhyolites, Owens et al. (2013) analyzed water concentrations in feldspar-hosted
467 melt inclusions in several samples; the highest value of 4.8 wt% was found in an explosively
468 erupted unit. This maximum value for the melt water concentration in the Torfajökull rhyolites
469 provides an opportunity to use the plagioclase-liquid thermometer from this study to constrain
470 pre-eruptive temperatures. Given the range of plagioclase (An₂₇₋₁₅) observed in the Torfajökull
471 rhyolites, along with the range of whole-rock compositions (MacDonald et al., 1990), the
472 calculated pre-eruptive temperatures ranges from 780-830°C. These are minimum values, as
473 melt water concentrations \leq 4.8 wt% were measured in some of the units, and lower water
474 concentrations will lead to higher calculated temperatures. Nonetheless, the collective data
475 reveal that Icelandic rhyolites are surprisingly hydrous, with \leq 4.8 wt% H₂O in the Torfajökull
476 rhyolites (Owens et al., 2013) and \sim 3.5-3.6 wt% H₂O in the Thingmuli rhyolites (this study).

477
478

Implications and Recommended Applications

479 The plagioclase thermometer/hygrometer presented in this study is calibrated on a data
480 set that spans a wide range of liquid compositions (45-78 wt% SiO₂), including high-SiO₂
481 rhyolites and both metaluminous and alkaline liquids. In addition, the compositional range of
482 plagioclase in the calibration has been extended to values as sodic as An₁₇. It is demonstrated
483 that the updated hygrometer accurately reproduces plagioclase-liquid equilibrium experiments
484 that were conducted in a piston-cylinder apparatus at 1.0-1.2 GPa (Bartels et al., 1991), although
485 these experiments were not included in the calibration. This result shows that the updated
486 plagioclase-liquid hygrometer/thermometer in this study can be applied to all pressures

487 throughout the crustal column, and that the volumetric terms in the thermodynamic model
488 accurately account for the minor effect of pressure. Application of the revised plagioclase-liquid
489 hygrometer/thermometer is recommended for liquids that range from 45-78 wt% SiO₂,
490 plagioclase compositions that range from An₁₅₋₉₅, temperatures of 700-1300°C, and pressures of
491 0-1.2 GPa. The updated model can be downloaded in Excel format from the data repository or
492 obtained directly from the authors. The program is also available as a script formatted for MatLab
493 that may be obtained directly from the authors.

494

495 **ACKNOWLEDGEMENTS**

496 This study was supported by National Science Foundation grant (EAR-1250368). John
497 Naliboff is thanked for assistance and improvement upon the available MatLab script for the
498 plagioclase-hygrometer program. Thanks to Youxue Zhang and Ling Zeng for invaluable
499 feedback on the earlier 2009 version of this hygrometer, which led to important modifications.
500 We are particularly grateful for the thorough and constructive comments provided by Jim
501 Watkins, Julia Hammer and Chip Lesher, which led to an improved manuscript.

502

503 **REFERENCES**

- 504 Ai, Y. and Lange, R.A. (2008) New acoustic velocity measurements on CaO-MgO-Al₂O₃-SiO₂
505 liquids: Reevaluation of the volume and compressibility of CaMgSi₂O₆-CaAl₂Si₂O₈
506 liquids to 25 GPa. *Journal of Geophysical Research* 113, B04203, DOI:
507 10.1029/2007JB005010
- 508 Aigner-Torres, M., Blundy, J., Ulmer, P., Pettke, T. (2007) Laser ablation ICPMS study of trace
509 element partitioning between plagioclase and basaltic melts: an experimental approach.
510 *Contributions to Mineralogy and Petrology* 153, 647-667
- 511 Almeev, R. R., Bolte, T., Nash, B.P., Holtz, F., Erdmann, M. and Cathey, H. (2012) High-
512 temperature, low-H₂O silicic magmas of the Yellowstone Hotspot: an Experimental
513 Study of Rhyolite from the Bruneau-Jarbidge Eruptive Center, Central Snake River Plain,
514 USA. *Journal of Petrology* 53, 1837-1866
- 515 Anderson, A.T., Davis, A.M., and Lu, F. (2000) Evolution of Bishop Tuff Rhyolitic Magma

- 516 based on Melt and Magnetite Inclusions and Zoned Phenocrysts. *Journal of Petrology* 41,
517 449-473
- 518 Angel, R.J. (2004) Equations of state of plagioclase feldspars. *Contributions to Mineralogy and*
519 *Petrology* 146, 506–512
- 520 Bartels, K.S., Kinzler, R.J., and Grove, T.L. (1991) High pressure phase relations of primitive
521 high alumina basalts from Medicine Lake volcano, northern California. *Contributions to*
522 *Mineralogy and Petrology* 108, 253-270
- 523 Berman, R.G. (1988) Internally consistent thermodynamic data for minerals in the system Na₂O-
524 K₂O-CaO-MgO-FeO-Fe₂O₃-Al₂O₃-SiO₂-TiO₂-H₂O-CO₂. *Journal of Petrology* 29, 445–
525 522
- 526 Berndt, J., Koepke, J., and Holtz, F. (2005) An Experimental Investigation of the Influence of
527 Water and Oxygen Fugacity on Differentiation of MORB at 200 MPa. *Journal of*
528 *Petrology* 46, 135-167
- 529 Blatter, D. L. and Carmichael, I.S.E. (1998) Plagioclase-free andesites from Zitácuaro
530 (Michoacán), Mexico: Petrology and experimental constraints. *Contributions to*
531 *Mineralogy and Petrology* 231, 121-138
- 532 Blatter, D. L. and Carmichael, I.S.E. (2001) Hydrous phase equilibria of a Mexican high-silica
533 andesite: a candidate for mantle origin? *Geochimica et Cosmochimica Acta* 65, 4043-
534 4064
- 535 Blundy, J. (1997) Experimental study of a Kiglapait marginal rock and implications for trace
536 element partitioning in layered intrusions. *Chemical Geology* 141, 73-92
- 537 Boettcher, A.L., Burnham, C.W., Windown, K.E., and Bohlen, S.R. (1982) Liquids, glasses and
538 the melting of silicates to high pressures. *The Journal of Geology* 90, 127–138
- 539 Botcharnikov, R.E., Almeev, R.R., Koepke, J. and Holtz, F. (2008) Phase Relations and Liquid
540 Lines of Descent in Hydrous Ferrobasalt. Implications for the Skaergaard Intrusion and
541 Columbia River Flood Basalts. *Journal of Petrology* 49, 1687-1727
- 542 Brugger, C.R., Johnston, A.D. and Cashman, K.V. (2003) Phase relations in silicic systems at
543 one-atmosphere pressure. *Contributions to Mineralogy and Petrology* 146, 356-369
- 544 Carmichael, I.S.E. (1964) The petrology of Thingmuli, a Tertiary Volcano in Eastern Iceland.
545 *Journal of Petrology* 5, 435-460
- 546 Carmichael, I.S.E. (1967) The mineralogy of Thingmuli, A tertiary volcano in eastern Iceland.
547 *The American Mineralogist* 52, 1815-1841
- 548 Carmichael, I.S.E., Nicholls, J., Spera, F.J., Wood, B.J., and Nelson, S.A. (1977) High-
549 temperature properties of silicate liquids: Applications to the equilibration and ascent of
550 basic magma. *Philosophical Transactions of the Royal Society of London, Series A* 286,
551 373–431
- 552 Castro, J.M., Schipper, C.I., Mueller, S.P., Militzer, A.S., Amigo, A., Parejas, C., and Jacob, D.
553 (2013) Storage and eruption of near-liquidus rhyolite magma Cordón Caulle, Chile.
554 *Bulletin of Volcanology* 75, 701-718
- 555 Chesner, C.A. (1998) Petrogenesis of the Toba Tuffs, Sumatra, Indonesia. *Journal of Petrology*
556 49 397-438
- 557 Chesner, C.A. and Luhr, J.F. (2010) A melt inclusion study of the Toba Tuffs, Sumatra,
558 Indonesia. *Journal of Volcanology and Geothermal Research* 197, 259-278
- 559 Chesner, C.A. and Rose, W.I. (1991) Stratigraphy of the Toba Tuffs and evolution of the Toba
560 Caldera Complex, Sumatra, Indonesia. *Bulletin of Volcanology* 53, 343–356
- 561 Coombs, M.L. and Gardner, J.E. (2001) Shallow-storage conditions for the rhyolite of th 1912

- 562 eruption at Novarupta, Alaska. *Geology* 29, 775-778
- 563 Costa, F., Scaillet, B., and Pichavant, M. (2004) Petrological and experimental constraints on the
564 pre-eruptive conditions of Holocene dacite from Volcán San Pedro (36°S, Chilean
565 Andes) and the importance of sulphur in silicic subduction magmas. *Journal of Petrology*
566 45, 855-881
- 567 Couch, S., Harford, C.L., Sparks, R.S.J., and Carroll, M. R. (2003) Experimental constraints on
568 the formation of highly calcic plagioclase microlites at the Soufriere Hills Volcano,
569 Montserrat. *Journal of Petrology* 44, 1455-1475.
- 570 Danyushevksy, L.V., Carroll, M.R., and Falloon, T.J. (1997) Origin of high-An plagioclase in
571 Tongan high-Ca boninites: Implications for plagioclase-melt equilibria at low P(H₂O).
572 *The Canadian Mineralogist*, 35, 313–326
- 573 Draper, D.S. and Johnston, A.D. (1992) Anhydrous P-T phase relations of an Aleutian high-
574 MgO basalt: An investigation of the role of olivine-liquid reaction in the generation of arc
575 high-alumina basalts. *Contributions to Mineralogy and Petrology* 112, 501-519
- 576 Fei, Y. (1995) Thermal expansion. In T. Ahrens, Ed., *Mineral Physics and Crystallography*, p.
577 29–44 AGU Reference Shelf 2, Washington, D.C.
- 578 Gansecki, C.A. (1998) ⁴⁰Ar/³⁹Ar geochronology and pre-eruptive geochemistry of the
579 Yellowstone Plateau volcanic field rhyolites Ph.D. thesis, Stanford University
- 580 Gardner, J.E., Rutherford, M., Carey, S., and Sigurdsson, H. (1995) Experimental constraints on
581 pre-eruptive water contents and changing magma storage prior to explosive eruptions of
582 Mount St. Helens volcano. *Bulletin of Volcanology*, 57, 1-17.
- 583 Gardner, J.E., Layer, P.W. and Rutherford, M.J. (2002) Phenocrysts versus xenocrysts in the
584 youngest Toba Tuff: Implications for the petrogenesis of 2800 km³ of magma. *Geology*
585 30 347-350
- 586 Geschwind, C.H. and Rutherford, M.J. (1995) Crystallization of microlites during magma ascent:
587 the fluid mechanics of 1980-1986 eruptions at Mount St. Helens. *Bulletin of Volcanology*
588 57, 356-370
- 589 Ghiorso, Mark S., Hirschmann, Marc M., Reiners, Peter W., and Kress, Victor C. III (2002) The
590 pMELTS: An revision of MELTS aimed at improving calculation of phase relations and
591 major element partitioning involved in partial melting of the mantle at pressures up to 3
592 GPa. *Geochemistry, Geophysics Geosystems* 3(5), 10.1029/2001GC000217
- 593 Ghiorso, M. and Evans, B.W. (2008) Thermodynamics of rhombohedral oxide solid solutions
594 and a revision of the Fe-Ti two-oxide geothermometer and oxygen barometer. *American*
595 *Journal of Science* 308, 957-1039
- 596 Glazner, A.F. (1984) Activities of olivine and plagioclase components in silicate melts and their
597 application to geothermometry. *Contributions to Mineralogy and Petrology*, 88, 260–268
- 598 Grove, T.L. Gerlach, D.C. and Sando, T.W. (1982) Origin of calc-alkaline series lavas at
599 Medicine Lake volcano by fractionation, assimilation and mixing. *Contributions to*
600 *Mineralogy and Petrology* 80, 160-182
- 601 Grove, T.L., Bryan, W.B. (1983) Fractionation of pyroxene-phyric MORB at low pressure: an
602 experimental study. *Contributions to Mineralogy and Petrology* 84, 293-309
- 603 Grove, T. L. and Juster, T.C. (1989) Experimental investigations of low-Ca pyroxene stability
604 and olivine-pyroxene-liquid equilibria at 1 atm in natural basaltic and andesitic liquids.
605 *Contributions to Mineralogy and Petrology* 103, 287-305
- 606 Grove, T.L., Donnelly-Nolan, J.M. and Housh, T. (1997) Magmatic processes that generated the
607 rhyolite of Glass Mountain, Medicine Lake volcano, N. California. *Contributions to*

- 608 Mineralogy and Petrology 127, 205-223
- 609 Grove, T.L., Elkins-Tanton, L.T., Parman, S.W., Catterjee, N., Mütener, O., Gaetani, G.A.
610 (2003) Fractional crystallization and mantle-melting controls on calc-alkaline
611 differentiation trends. *Contributions to Mineralogy and Petrology* 145, 515-533
- 612 Gualda G.A.R., Ghiorso M.S., Lemons R.V., Carley T.L. (2012) Rhyolite-MELTS: A modified
613 calibration of MELTS optimized for silica-rich, fluid-bearing magmatic systems. *Journal*
614 *of Petrology* 53, 875-890
- 615 Hildreth, W. (1977) The magma chamber of the Bishop Tuff: gradients in temperature, pressure,
616 and composition. Ph.D. thesis, University of California, Berkeley
- 617 Hildreth, W. and Wilson, C.J.N. (2007) Compositional Zoning of the Bishop Tuff. *Journal of*
618 *Petrology* 48, 951-999
- 619 Holland, T. and Powell, R. (1992) Plagioclase feldspars: Activity-composition relations based
620 upon Darken's quadratic formalism and Landau theory. *American Mineralogist* 77, 53-61
- 621 Holtz, R., Johannes, W., Tamic, N., and Behrens, H. (2005) Experimental petrology of the 1991-
622 1995 Unzen dacite, Japan. Part I: phase relations, phase composition and pre-eruptive
623 conditions. *Journal of Petrology* 46, 319-337
- 624 Housh, T.B. and Luhr, J.F. (1991) Plagioclase-melt equilibria in hydrous systems. *American*
625 *Mineralogist* 76, 477-492
- 626 Hamada, M. and Fujii, T. (2008) Experimental constraints on the effects of pressure and H₂O on
627 the fractional crystallization of high-Mg island arc basalt. *Contributions to Mineralogy*
628 *and Petrology* 155, 767-790
- 629 Holland, T. and Powell, R. (1992) Plagioclase feldspars: Activity-composition relations based
630 upon Darken's quadratic formalism and Landau theory. *American Mineralogist*, 77, 53-
631 61.
- 632 Irvine, T.N. and Baragar, W.R.A. (1971) A guide to the chemical classification of the common
633 volcanic rocks. *Canadian Journal of Earth Sciences* 8, 523-548
- 634 Juster, T. C., Grove, T. and Perfit, M. R. (1989) Experimental constraints on the generation of
635 Fe-Ti basalts, andesites and rhyodacites at the Galapagos spreading center 85°W and
636 95°W. *Journal of Geophysical Research*, 94, 9251-9274
- 637 Kress, V.C., Williams, Q., and Carmichael, I.S.E. (1988) Ultrasonic investigation of melts in the
638 system Na₂O-Al₂O₃-SiO₂. *Geochimica et Cosmochimica Acta* 52, 283-293
- 639 Kudo, A.M. and Weill, D.F. (1970) An igneous plagioclase thermometer. *Contributions to*
640 *Mineralogy and Petrology*, 25, 52-65.
- 641 Lange, R.A. (1996) Temperature independent thermal expansivities of sodium aluminosilicate
642 melts between 713 and 1835 K. *Geochimica et Cosmochimica Acta* 60, 4989-4996
- 643 ——— (1997) A revised model for the density and thermal expansivity of K₂O-Na₂O-CaO-
644 MgO-Al₂O₃-SiO₂ liquids from 700 to 1900 K: Extension to crustal magmatic
645 temperatures. *Contributions to Mineralogy and Petrology* 130, 1-11
- 646 ——— (2003) The fusion curve of albite revisited and the compressibility of NaAlSi₃O₈ liquid
647 with pressure. *American Mineralogist* 88, 109-120
- 648 Lange, R. A., Frey, H. M. and Hector, J. (2009) A thermodynamic model for the plagioclase-
649 liquid hygrometer/thermometer. *American Mineralogist* 94, 494-506
- 650 Larsen, J.F. (2005) Experimental study of plagioclase rim growth around anorthite seed crystals
651 in rhyodacitic melt. *American Mineralogist* 90, 417-427
- 652 Larsen, J.F. (2006) Rhyodacite magma storage conditions prior to the 3430y BP caldera-forming
653 eruption of Aniakchak volcano, Alaska. *Contributions to Mineralogy and Petrology* 152,

- 654 523-540
655 Lowenstern, J.B. (1993), Evidence for Cu-bearing fluid in magma erupted at the Valley of Ten
656 Thousand Smokes, Alaska. *Contributions to Mineralogy and Petrology* 114, 409-421
657 Luhr, J.F. (1990) Experimental phase relations of water- and sulfur-saturated arc magmas and the
658 1982 eruptions of El Chichón volcano. *Journal of Petrology* 31, 1071–1114
659 MacDonald, R., McGarvie, D.W., Pinkerton, H., Smith, R.L. and Palacz, Z.A. (1990)
660 Petrogenetic Evolution of the Torfajökull Volcanic Complex, Iceland I. Relationship
661 Between the Magma Types. *Journal of Petrology* 31, 429-459
662 Mahood, G.A. and Baker, D.R. (1986) Experimental constraints on depths of fractionation of
663 mildly alkalic basalts and associated felsic rocks: Pantelleria, Strait of Sicily.
664 *Contributions to Mineralogy and Petrology* 93, 251-264
665 Marsh, B.D., Fournelle, J., Myers, J.D., and Chou, I.-M. (1990) On plagioclase thermometry in
666 island-arc rocks: Experiments and theory. In R.J. Spencer and I.-M. Chou, Eds., *Fluid-
667 Mineral Interactions: a Tribute to H.P. Eugster*, 2, p. 65–83. *Geochemical Society Special
668 Publication*, St. Louis, Missouri
669 Martel, C., Pichavant, M., Holtz, F., and Scaillet, B. (1999) Effects of fO_2 and H_2O on andesite
670 phase relations between 2 and 4 kbar. *Journal of Geophysical Research*, 104, 29453–
671 29470.
672 Martel, C. & Schmidt, B.C., (2003) Decompression experiments as an insight into ascent rates of
673 silicic magmas. *Contributions to Mineralogy and Petrology* 144, 397-415
674 Martel, C. (2012) Eruption Dynamics inferred from microlite crystallization experiments:
675 Application to Plinian and Dome-forming Eruptions of Mt. Pelée (Martinique, Lesser
676 Antilles). *Journal of Petrology* 53, 699-725
677 Martel, C., Champallier, R., Prouteau, G., Pichavant, M., Arbaret, L., Balcone-Boissard, H.,
678 Boudon, G., Boivin, P., Bourdier, J., Scaillet, B. (2013) Trachyte Phase Relations and
679 Implication for Magma Storage Conditions in the Chaîne des Puys (French Massif
680 Central). *Journal of Petrology* 54, 1071-1107
681 Mathez, E.A. (1973) A refinement of the Kudo-Weill plagioclase thermometer and its
682 application to basaltic rocks. *Contributions to Mineralogy and Petrology* 41, 61–72
683 Metz, J.M. and Mahood, G.A. (1991) Development of the Long Valley, California, magma
684 chamber recorded in precaldera rhyolite lavas of Glass Mountain. *Contributions to
685 Mineralogy and Petrology* 106, 379-397
686 Moore, G. (2008) Interpreting H_2O and CO_2 contents in melt inclusions: Constraints from
687 solubility experiments and modeling. In K.D. Putirka and F.J. Tepley III, Eds., *Minerals,
688 Inclusions and Volcanic Processes* 69, p. 333–361 *Reviews in Mineralogy and
689 Geochemistry*, Mineralogical Society of America, Chantilly, Virginia
690 Moore, G. and Carmichael, I.S.E. (1998) The hydrous phase equilibria (to 3 kbar) of an andesite
691 and basaltic andesite from western Mexico: constraints on water content and conditions
692 of phenocryst growth. *Contributions to Mineralogy and Petrology*, 130, 304–319
693 Moore, G., Vennemann, T., and Carmichael, I.S.E. (1998) An empirical model for the solubility
694 of water in magmas to 3 kbars. *American Mineralogist*, 83, 36–42
695 Owen, J., Tuffen, H. and McGarvie, D.W. (2013) Explosive subglacial rhyolitic eruptions in
696 Iceland are fuelled by high magmatic H_2O and closed-system degassing. *Geology* 41,
697 251-254
698 Panjasawatwong, Y., Danyushevsky, L.V., Crawford, A.J., and Harris, K.L. (1995) An
699 experimental study of the effects of melt composition on plagioclase-melt equilibria at 5

- 700 and 10 kbar; implications for the origin of magmatic high-An plagioclase. Contributions
701 to Mineralogy and Petrology, 118, 420–432
- 702 Parman, S.W., Grove, T.L., Kelley, K.A., and Plank, T. (2011) Along-Arc Variations in the Pre-
703 Eruptive H₂O Contents of Mariana Arc Magmas Inferred from Fractionation Paths.
704 Journal of Petrology 52, 257-278
- 705 Putirka K.D. (2005) Igneous thermometers and barometers based on plagioclase + liquid
706 equilibria: Tests of some existing models and new calibrations. American Mineralogist
707 90, 336–346
- 708 ——— (2008) Thermometers and barometers for volcanic systems, in: Putirka, K. D., and
709 Tepley, F. eds., Reviews in Mineralogy and Geochemistry vol. 69, p 61-120
- 710 Rader, E. L. and Larsen, J.F. Experimental phase relations of a low MgO Aleutian basaltic
711 andesite at XH₂O 5 0.7–1. Contributions to Mineralogy and Petrology, 166, 1593-1611
- 712 Rankin, G.A. and Wright, F.E. (1915) The ternary system CaO-Al₂O₃-SiO₂. American Journal of
713 Science, 39, 1–79
- 714
- 715 Richet, P. and Bottinga, Y. (1984a) Glass transitions and thermodynamic properties of
716 amorphous SiO₂, NaAlSi₃O₈, and KAlSi₃O₈ Geochimica et Cosmochimica Acta 48,
717 453–470.
- 718 Richet, P. and Bottinga, Y. (1984b) Anorthite, andesine, wollastonite, diopside, cordierite, and
719 pyrope: Thermodynamics of melting, glass transitions, and properties of the amorphous
720 phases. Earth and Planetary Science Letters 67, 415-432
- 721 Sack, R.O., Walker, D. and Carmichael, I.S.E. (1987) Experimental petrology of alkalic lavas:
722 constraints on cotectics of multiple saturation in natural basic liquids. Contributions to
723 Mineralogy and Petrology 96, 1-23
- 724 Scaillet, B. and Evans, B. W. (1999) The 15 June 1991 eruption of mount Pinatubo. I. Phase
725 equilibria and pre-eruption P-T-fO₂-fH₂O conditions of the dacite magma. Journal of
726 Petrology 40, 381-411
- 727 Shea, T. and Hammer, J.E. (2013) Kinetics of cooling- and decompression-induced
728 crystallization in hydrous mafic-intermediate magmas. Journal of Volcanology and
729 Geothermal Research 260, 127-145
- 730 Sisson, T.W. and Grove, T.L. (1993a) Experimental investigations of the role of H₂O in calc-
731 alkaline differentiation and subduction zone magmatism. Contributions to Mineralogy
732 and Petrology 113, 143–166
- 733 ——— (1993b) Temperatures and H₂O contents of low-MgO high-alumina basalts.
734 Contributions to Mineralogy and Petrology 113, 167–184
- 735 Snyder, D., Carmichael, I.S.E., and Wiebe, R.A. (1993) Experimental study of liquid evolution
736 in a Fe-rich, layered mafic intrusion: constraints of Fe-Ti oxide precipitation on the *T-fO₂*
737 and *T-P* paths of tholeiitic magmas. Contributions to Mineralogy and Petrology 113, 73–
738 86
- 739 Stebbins, J.F., Carmichael, I.S.E., and Weill, D.E. (1983) The high temperature liquid and glass
740 heat contents and heats of fusion of diopside, albite, sanidine, and nepheline. American
741 Mineralogist 68, 717–730
- 742 Takagi, D., Sato, H. and Nakagawa, M. (2005) Experimental study of a low-alkali tholeiite at 1-5
743 kbar: optimal condition for the crystallization of high-An plagioclase in hydrous arc
744 tholeiite. Contributions to Mineralogy and Petrology 149, 527-540
- 745 Tenner, T.J., Lange, R.A., and Downs, R.T. (2007) The albite fusion curve reexamined: New

- 746 experiments and the high-pressure density and compressibility of high albite and
747 NaAlSi₃O₈ liquid. *American Mineralogist* 92, 1573–1585
- 748 Thy P., Leshner, C.E., Nielsen, T.F. and Brooks, C.K. (2006) Experimental constraints on the
749 Skaergaard liquid line of descent. *Lithos* 92,154-180
- 750 Tomiya, A., Takahashi, E., Furukawa, N., and Suzuki, T. (2010) Depth and Evolution of a Silicic
751 Magma Chamber: Melting Experiments of a Low-K Rhyolite from Usu Volcano, Japan.
752 *Journal of Petrology* 51, 1333-1354
- 753 Toplis, M.J., Libourel, G. and Carroll, M.R. (1994) The role of phosphorous in crystallization
754 processes of basalt: An experimental study. *Geochimica Cosmochimica Acta* 58, 797-810
- 755 Toplis, M.J. and Carroll, M.R. (1995) An experimental study of the influence of oxygen fugacity
756 on Fe-Ti oxide stability, phase relations, and mineral/melt equilibria in ferro-basaltic
757 systems. *Journal of Petrology* 36, 1137-1170
- 758 Tormey, D.R., Grove, T.L., and Bryan, W.B. (1987) Experimental petrology of normal MORB
759 near the Kane Fracture Zone: 22–25° N, mid-Atlantic ridge. *Contributions to Mineralogy
760 and Petrology* 96, 121–139
- 761 Vander Auwera, J., Longhi, J. and Duchesne, J.C. (1998) A liquid line of descent of the jotunite
762 (hypersthene monzodiorite) suite. *Journal of Petrology* 39, 439-468
- 763 Wagner, T.P., Donnelly-Nolan, J.M., and Grove, T.L. (1995) Evidence of hydrous differentiation
764 and accumulation in the low-MgO, high-Al₂O₃ Lake Basalt from Medicine Lake
765 volcano, California. *Contributions to Mineralogy and Petrology* 121, 201–216
- 766 Wainright, J.E. and Starkey, J. (1971) A refinement of the crystal structure of anorthite.
767 *Zeitschrift für Kristallographie*, 133, 75–84
- 768 Wallace, P.J., Anderson, A.T. and Davis, A.M. (1999) Gradients in H₂O, CO₂, and exsolved gas
769 in a large-volume silicic magmas system: Interpreting the record preserved in melt
770 inclusions from the Bishop Tuff. *Journal of Geophysical Research* 104, 97-122
- 771 Wallace, P. (2005) Volatiles in subduction zone magmas: concentrations and fluxes based on
772 melt inclusion and volcanic gas data. *Journal of Volcanology and Geothermal Reseach.*
773 140, 217-240
- 774 Waters, L.E., Andrews, B.J., and Lange, R.A. (in review) Degassing-induced crystallization of
775 plagioclase phenocrysts in rhyolite and dacite: Phase equilibrium and decompression
776 experiments: *Journal of Petrology*
- 777 Watson, E.B. and Harrison, T.M. (1983) Zircon saturation revisited: temperature and
778 composition effects in a variety of crustal magma types. *Earth and Planetary Science
779 Letters* 64, 295-304
- 780 Watts K. E., Bindeman, I.N. and Schmitt, A.K. (2011) Large-volume rhyolite genesis in caldera
781 complexes of the Snake River Plain: insights from the Kilgore Tuff of the Heise volcanic
782 field, Idaho, with comparison to Yellowstone and Bruneau-Jarbidge rhyolites. *Journal of
783 Petrology* 52, 857-890
- 784 Wruck, B., Salje, E.K.H., and Graeme-Barber, A. (1991) Kinetic rate laws derived from order
785 parameter theory IV: Kinetics of Al,Si disordering in Na-feldspars. *Physics and
786 Chemistry of Minerals*, 17, 700–710
- 787 Yang, H.J., Kinzler, R.J. and Grove, T.L. (1996) Experiments and models of anhydrous basaltic
788 olivine-plagioclase-augite saturated melts from 0.001 to 10 kbar. *Contributions to
789 Mineralogy and Petrology* 124, 1-18
- 790 Zeng, L., Cheng, L. Cheng, Q., and Zhang, S. (2014) A refinement of Lange's plagioclase–liquid
791 hygrometer/thermometer based on quadratic log-contrast models for experiments with

792 mixtures. Journal of Geochemical Exploration 141, 89-99
793 Zhang, Y., Xu, Z., Zhu, M., and Wang, H. (2007) Silicate melt properties and volcanic eruptions.
794 Reviews of Geophysics 45, RG4004
795

796 **Figure Captions**

797

798 **Figure 1:** (A) Histogram of hydrous (light grey) and anhydrous (black) liquid compositions used
799 in the calibration of the hygrometer as a function of wt% SiO₂ in the melt. (B) A histogram of
800 plagioclase compositions used in the calibration of the hygrometer as a function of mol% An.

801

802 **Figure 2:** Plot showing the range in total alkali content (wt% Na₂O + wt% K₂O) as a function of
803 wt% SiO₂ for liquids used in the calibration of the hygrometer, along with the proposed
804 boundary between alkaline and calc-alkaline liquids from Irvine & Baragar (1972). Water-
805 saturated experiments are shown as hollow circles, anhydrous experiments are shown as black
806 diamonds, and the experiments used in the calibrations Lange et al. (2009) are shown as grey
807 circles.

808

809 **Figure 3:** (A) Plot showing the experiments used in the calibration of the hygrometer as a
810 function of liquid An-number and mol% An in plagioclase. (B) Plot showing the experiments
811 used in the calibration of the hygrometer as a function of wt% SiO₂ in the liquid and mol%An in
812 plagioclase. The dashed lines highlight the limits of the calibration of Lange et al. (2009), which
813 does not adequately cover the liquids with low An-numbers (rhyolitic). Symbols the same as in
814 Fig. 2.

815

816 **Figure 4:** (A) A plot of measured water contents from the calibration v. the predicted water
817 contents derived from the hygrometer, with a 1:1 correspondence line, and dashed lines
818 reflecting two standard errors (± 0.7 wt% H₂O). (B) Results of the plagioclase-liquid hygrometer
819 show as a function of residuals (measured wt% H₂O – predicted wt% H₂O). With the exception
820 of three experiments, the hygrometer predicts melt water contents for the calibration data set
821 within <1 wt%.

822

823 **Figure 5:** The residuals (measured – predicted wt% H₂O) of the hygrometer plotted against (A)
824 wt% SiO₂, (B) Total Alkalis (wt% Na₂O + wt% K₂O), (C) liquid An-number, (D) plagioclase
825 composition (mol% An), (E) temperature (°C), and (F) melt viscosity (log₁₀ Pa s). In all plots
826 (A-F), water saturated experiments are shown as hollow circles, anhydrous experiments are
827 shown as black diamonds. For comparison, results from the model of Lange et al. (2009) are
828 shown as grey circles.

829

830 **Figure 6:** (A) Comparison of measured vs. predicted temperature (°C) using a 1:1
831 correspondence line. The average difference is 12°C (14°C and 10°C for hydrous and anhydrous
832 experiments, respectively). Also shown are dashed lines marking $\pm 40^\circ\text{C}$, which highlights that
833 the model recovers temperatures within $\leq 40^\circ\text{C}$ for 210 of 214 experiments. (B) The difference in
834 measured vs. predicted temperature for the calibration data set, shown as a histogram.

835

836 **Figure 7:** The difference between measured and predicted temperature for the calibration data
837 set plotted against (A) wt% SiO₂, (B) temperature, and (C) wt% H₂O. In all plots (A-C), water
838 saturated experiments are shown as hollow circles, and anhydrous experiments are shown as
839 black diamonds. For comparison, results from the thermometer of Putirka (2008) are shown as
840 grey diamonds in A-C.

841

842 **Figure 8:** A comparison of H₂O contents calculated by the plagioclase-liquid hygrometer on
843 H₂O under-saturated experiments in the studies of Almeev et al. (2012), Bartels et al. (1991) and
844 Hamada and Fujii (2008), where H₂O contents were measured using FTIR. Experiments of
845 Almeev et al. (2012) and Hamada and Fugii (2008) were conducted under mixed CO₂-H₂O
846 conditions on a rhyolite and basalt, respectively. Bartels et al. (1991) performed anhydrous
847 experiments on a basalt and in a piston cylinder at pressures ≥ 1 GPa. See text for discussion.
848

849 **Figure 9:** Measured minus predicted wt% H₂O, using the the plagioclase-liquid hygrometer, for
850 the anhydrous experiments on rhyolite liquid of Brugger et al. (2003) plotted as a function of
851 wt% SiO₂.
852

853 **Figure 10:** A plot showing the effect of wt% H₂O in melt on equilibrium plagioclase
854 composition for rhyolite, andesite and basalt (see text for discussion).
855

856 **Figure 11:** A plot showing the effect of pressure (MPa) on the wt% H₂O value calculated with
857 the plagioclase-liquid hygrometer for three liquids (rhyolite, andesite, and basalt). Horizontal
858 light-grey isopleths of 2, 4 and 6 wt% H₂O highlight the small effect of pressure. See text for
859 discussion.
860

861 **Figure 12:** (A) A plot of plagioclase composition (mol% An) as a function of temperature for 13
862 samples from the Bishop Tuff using the data reported in Hildreth (1977). (B) A plot showing
863 water contents for the Bishop Tuff calculated using the plagioclase-liquid hygrometer, using
864 plagioclase compositions from (A) and temperatures from Hildreth and Wilson (2007). Also
865 shown are reported water contents in melt inclusions from the Early (Ig1Eb), Middle (Ig2Ea) and
866 Late (Ig1NWa and Ig1NWb) units of the Bishop Tuff from Wallace et al. (1999) (black crosses)
867 and Anderson et al. (2000) (grey diamonds). The width of the grey boxes reflects the range of
868 reported temperatures for each unit in Hildreth and Wilson (2007). See text for discussion.
869

870 **Figure 13:** Application of the plagioclase-liquid hygrometer to the Youngest Toba Tuff (YTT),
871 using the plagioclase compositions, and bulk compositions reported in Chesner (1998). The pre-
872 eruptive temperatures presented for the YTT have been recalculated using the oxide
873 compositions presented in Chesner (1998) and the geo-thermometer of Ghiorso and Evans
874 (2008). The results of the hygrometer are shown as stars. Also shown are the phase equilibrium
875 experiments (grey circles) and mineral-in curves of Gardner et al. (2002), along with isopleths of
876 H₂O solubility (in wt %) for the YTT calculated with Zhang et al. (2007). The water contents
877 derived from the plagioclase-liquid hygrometer are consistent with the plagioclase-in curve of
878 Gardner et al. (2002). Also shown on the phase diagram is a grey field that shows the range of
879 reported water contents, 3.9-6.4 wt%, in quartz-hosted melt inclusions from Chesner and Luhr
880 (2010). The grey field is defined by pre-eruptive temperatures presented in Chesner (1998) and
881 the quartz-in curve as determined by Gardner et al. (2002). The water contents recorded by the
882 melt inclusions and the plagioclase-liquid hygrometer are consistent with the phase equilibrium
883 experiments. See text for discussion.
884

885 **Figure 14:** A plot showing estimates of minimum pre-eruptive temperatures (°C) that are
886 calculated by applying the plagioclase-liquid thermometer to 19 rhyolite lavas from the
887 Torfajökull Volcanic Complex, for which water contents (≤ 4.8 wt%) have been measured in melt

888 inclusions (Owen et al. 2013). Plagioclase compositions (An_{15} - An_{27}) are from MacDonald et al.
889 (1990). See text for discussion.

Table 1A. Summary of albite thermodynamic data used in the hygrometer model

Parameter	Value	Reference
T_f	1373 K	Boettcher et al. (1982)
$\Delta H_{fus}(T_f)$	64.5 kJ/(mol·K)	Tenner et al. (2007)
$\Delta S_{fus}(T_f)$	47.0 J/(mol·K)	Tenner et al. (2007)
C_p crystal	$393.64 - 2415.5T^{-0.5} - 7.8928 \cdot 10^6 T^{-2} + 1.07064 \cdot 10^9 T^{-3}$	Berman (1988)
C_p liquid	359 J/(mol·K)	Tenner et al. (2007)
V_{298K} crystal	100.57 cm ³ /mol	Wruck et al. (1991)
$\alpha(T)$ crystal	$2.68 \times 10^{-5} \text{ K}^{-1}$	Fei (1995)
$(\delta V/\delta P)^{crystal}$	-1.67 cm ³ /GPa	Tenner et al. (2007); Lange et al. (2009)
$V(T)$ liquid	$112.72 + 0.00382 (T-1373) \text{ cm}^3/\text{mol}$	Lange (1996)
$(\delta V/\delta P)^{liquid}$	$-6.379 - 0.00055 (T-1673) \text{ cm}^3/\text{GPa}$	Kress and Carmichael (1988)

Table 1B. Summary of anorthite thermodynamic data used in the hygrometer model

Parameter	Value	Reference
T_f	1830 K	Rankin and Wright (1915)
$\Delta H_{fus}(T_f)$	142.4 kJ/(mol·K)	This study (Appendix A)
$\Delta S_{fus}(T_f)$	77.8 J/(mol·K)	This study (Appendix A)
C_p crystal	$439.37 - 3734.1T^{-0.5} + 0.317024 \cdot 10^9 T^{-3}$	Berman (1988)
C_p liquid	433.6 J/(mol·K)	This study (Appendix A)
V_{298K} crystal	100.61 cm ³ /mol	Wainright and Starky (1971)
$\alpha(T)$ crystal	$1.41 \times 10^{-5} \text{ K}^{-1}$	Fei (1995)
$(\delta V/\delta P)^{crystal}$	-1.16 cm ³ /GPa	Angel (2004); Lange et al. (2009)
$V(T)$ liquid	$106.3 + 0.00371 (T-1673) \text{ cm}^3/\text{mol}$	Lange (1997)
$(\delta V/\delta P)^{liquid}$	$-5.182 - 0.00101 (T-1673) \text{ cm}^3/\text{GPa}$	Ai and Lange (2008)

<i>Table 2: Model Parameters</i>	<i>Fitted Values $\pm 1\sigma$</i>	<i>t-statistic</i>
a''	-17.3 \pm 2.53	-6.86
m'	0.39 \pm 0.12	3.40
b''	2.99 \pm 0.07	39.9
d'' (SiO ₂)	7.83 \pm 2.52	3.11
d'' (Al ₂ O ₃ *)	-50.1 \pm 3.53	-14.2
d'' (FeO ^T)	14.1 \pm 3.30	4.27
d'' (MgO)	24.0 \pm 3.05	7.86
d'' (CaO)	-15.9 \pm 3.45	-4.61
d'' (Na ₂ O)	18.6 \pm 4.32	4.31
d'' (K ₂ Al ₂ O ₄)	24.0 \pm 6.73	3.57

Number of cases = 214; SEE = 0.35 wt% H₂O; R² = 0.98

*Al₂O₃ is moles Al₂O₃ minus the moles of K₂O

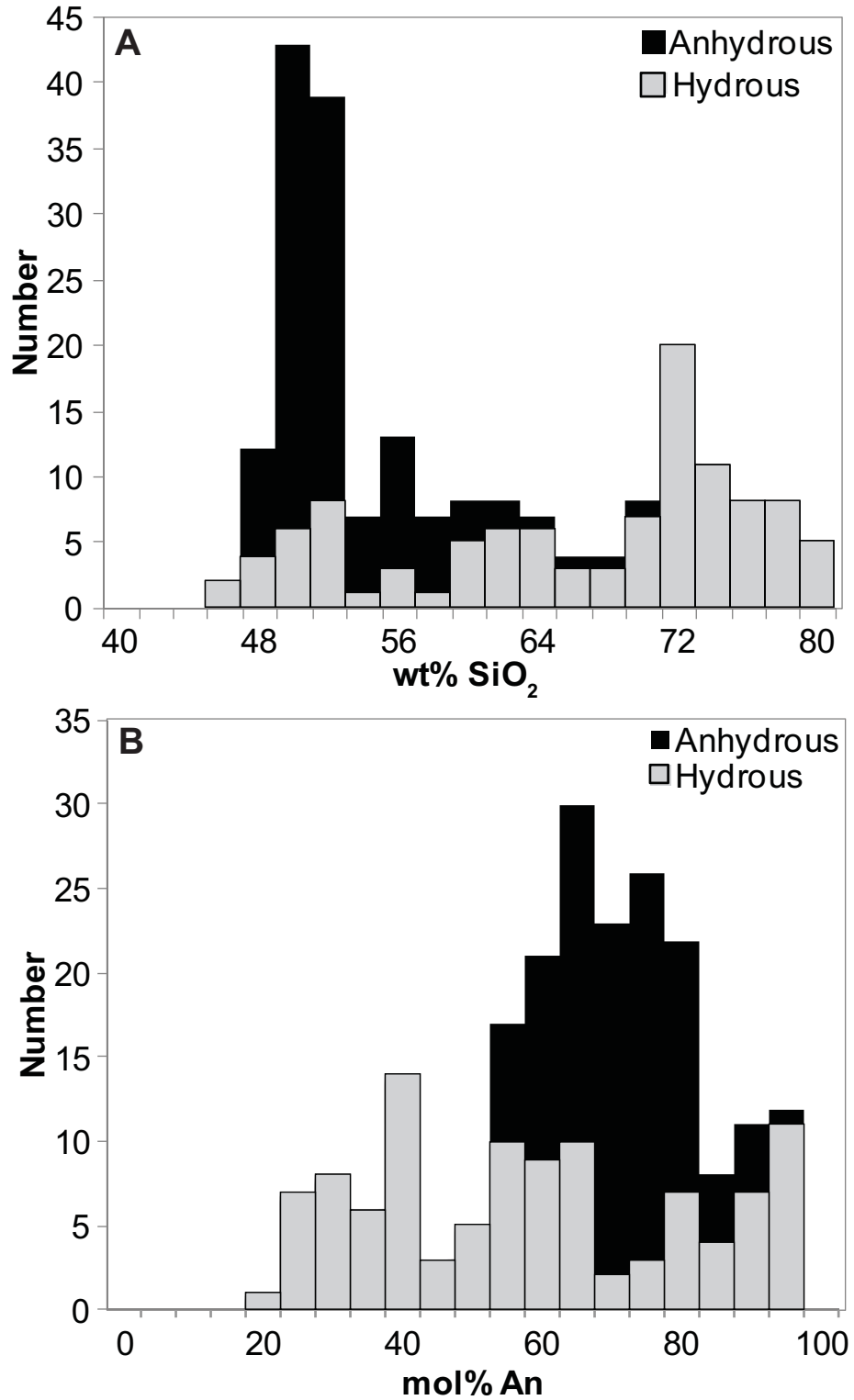


Figure 1

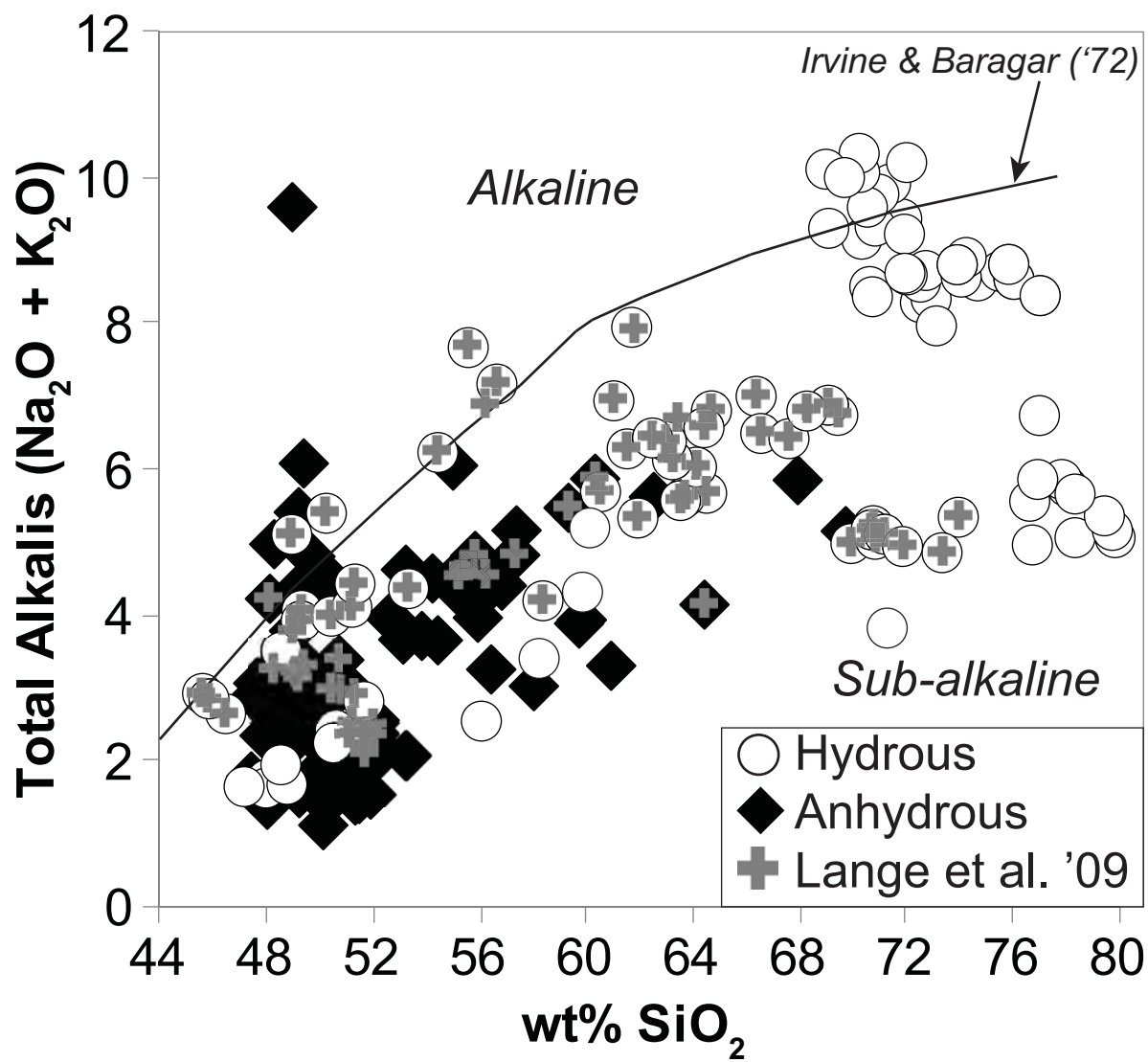


Figure 2

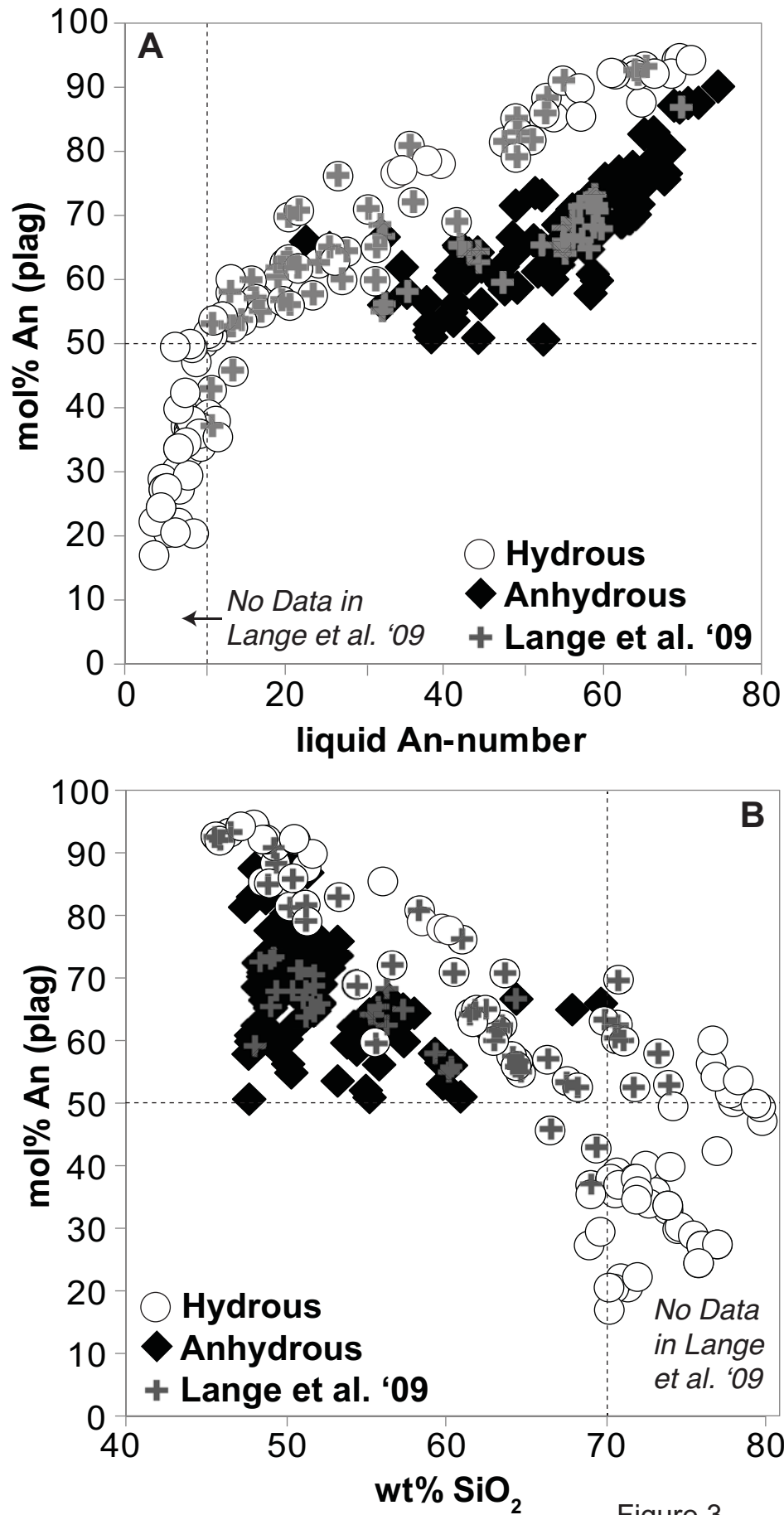


Figure 3

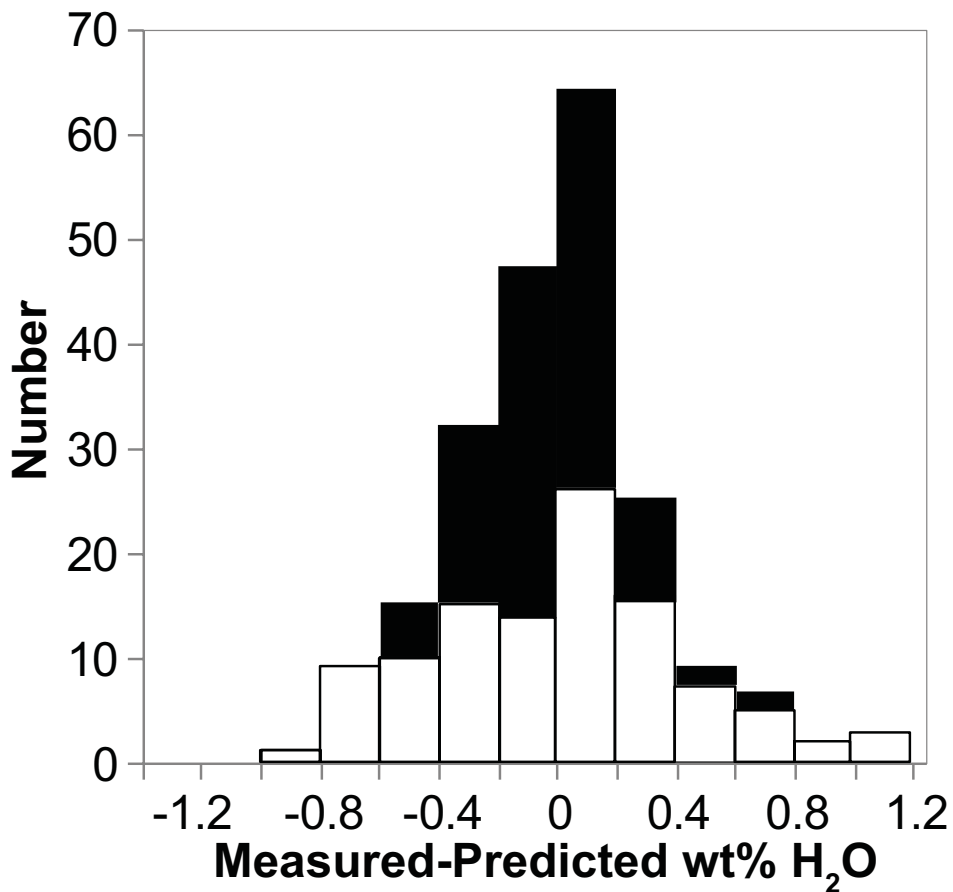
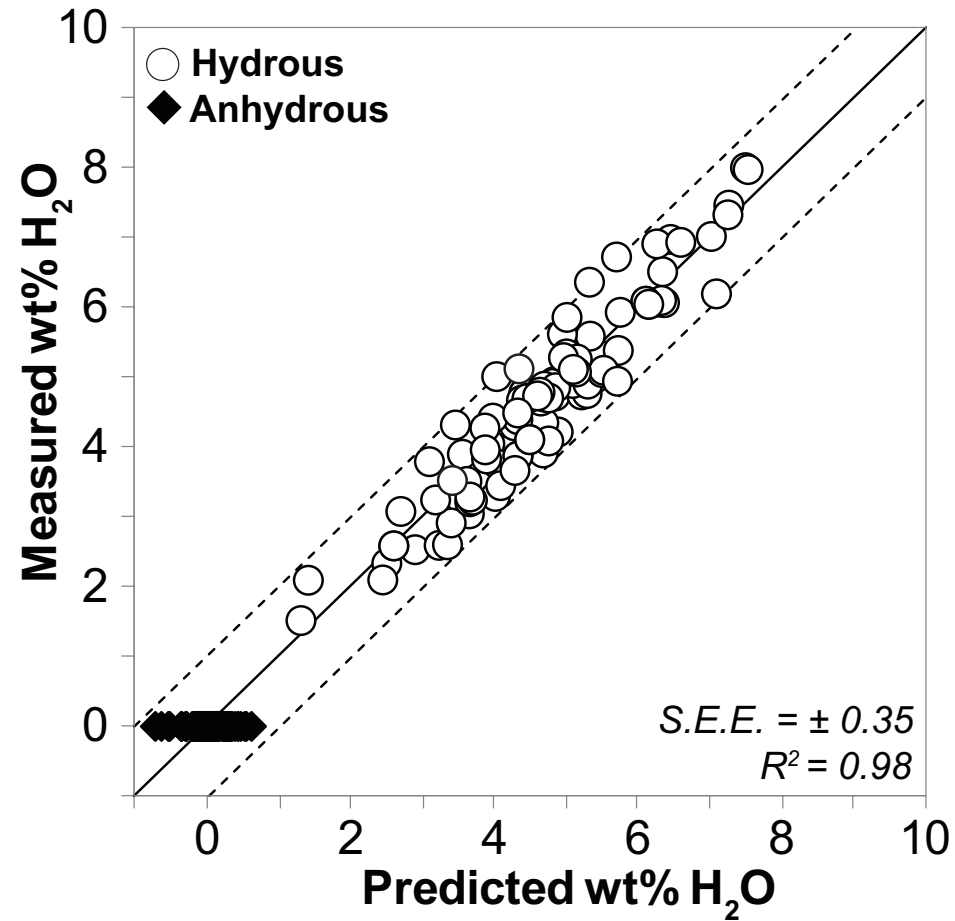


Figure 4

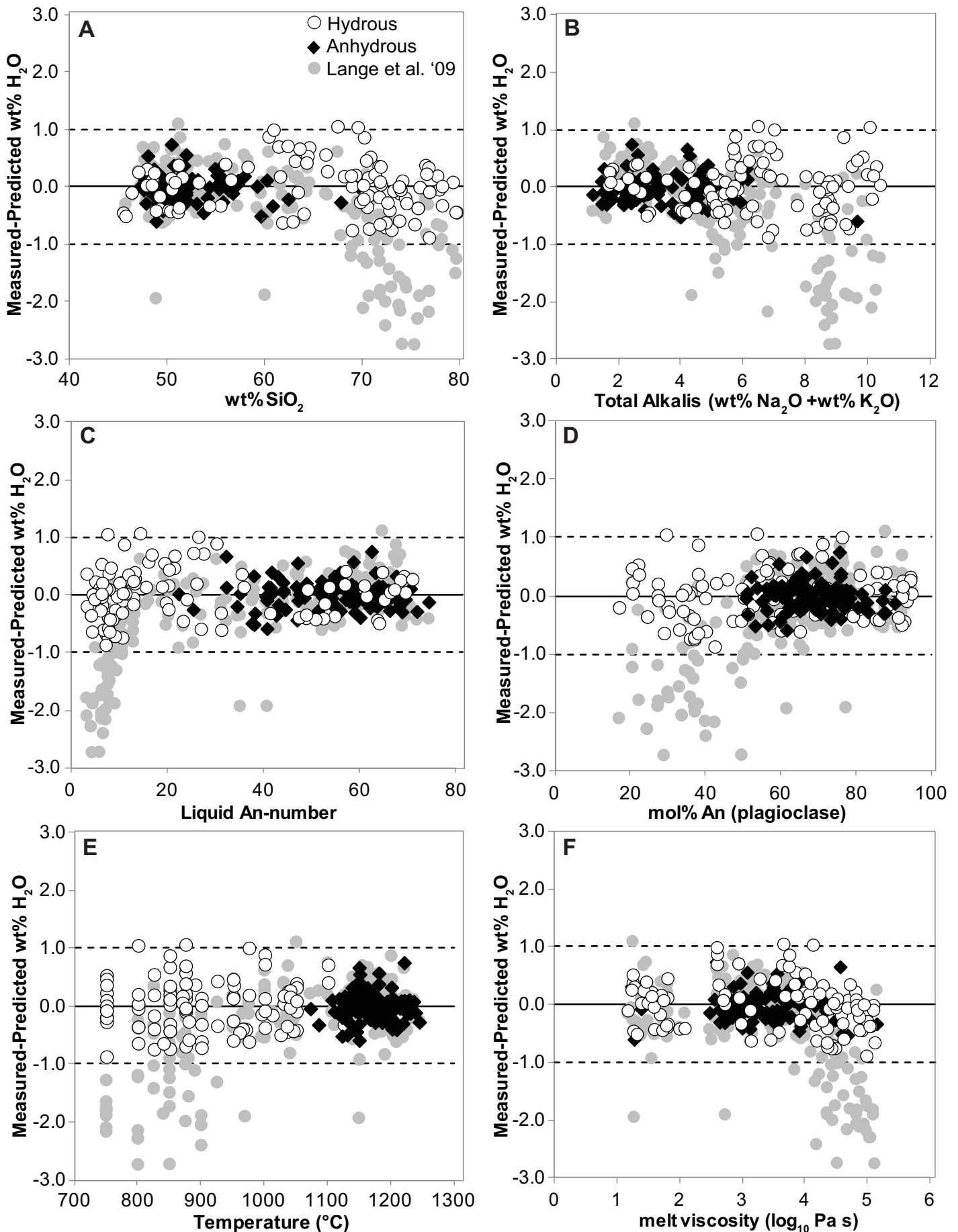


Figure 5

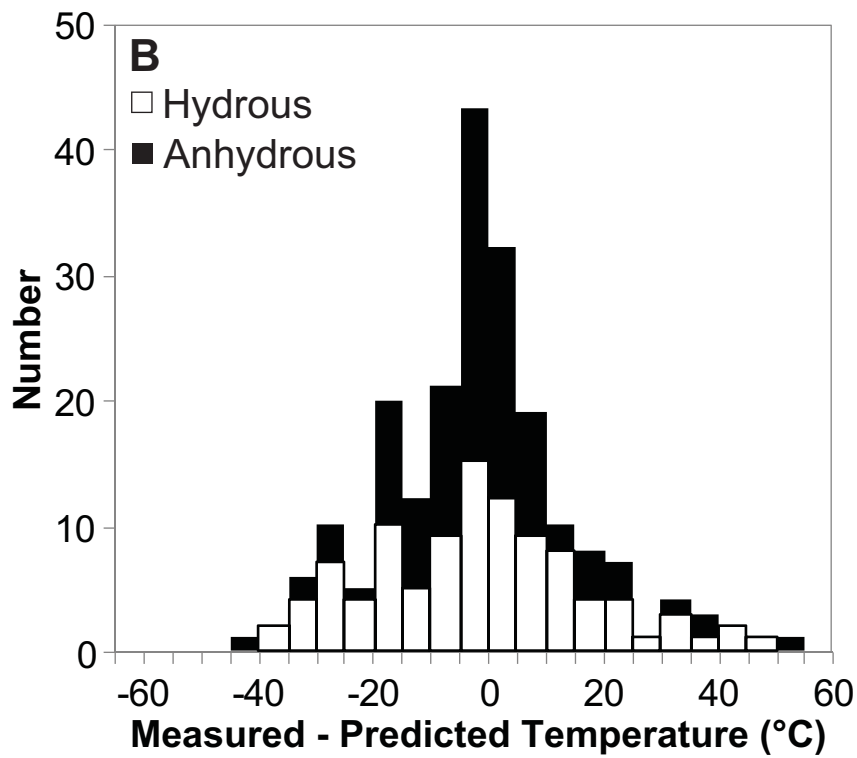
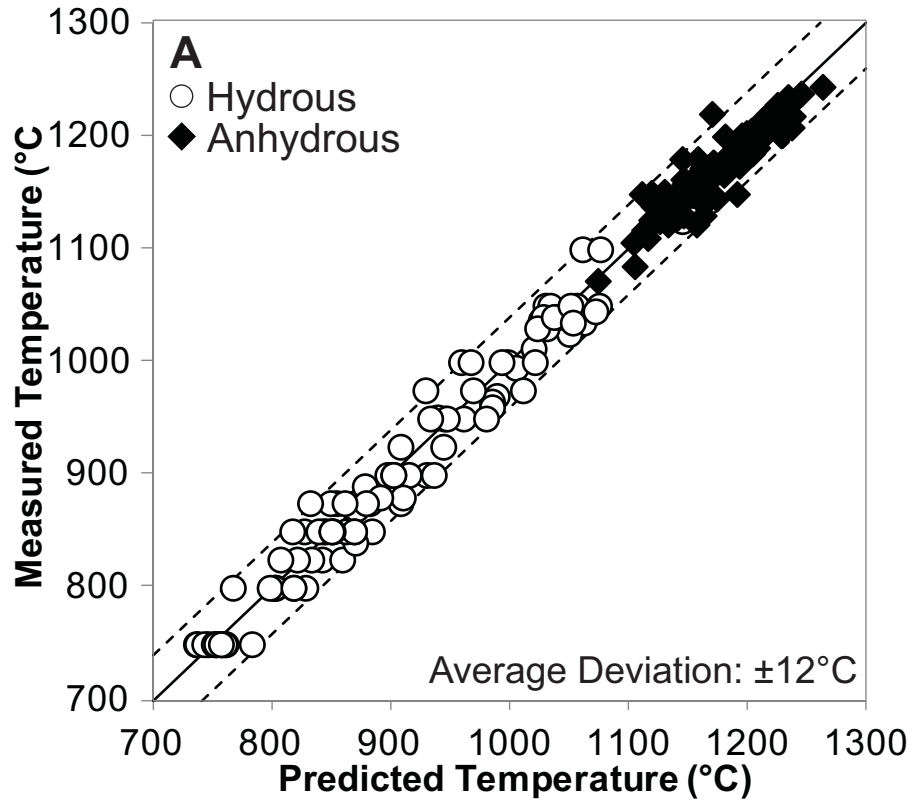


Figure 6

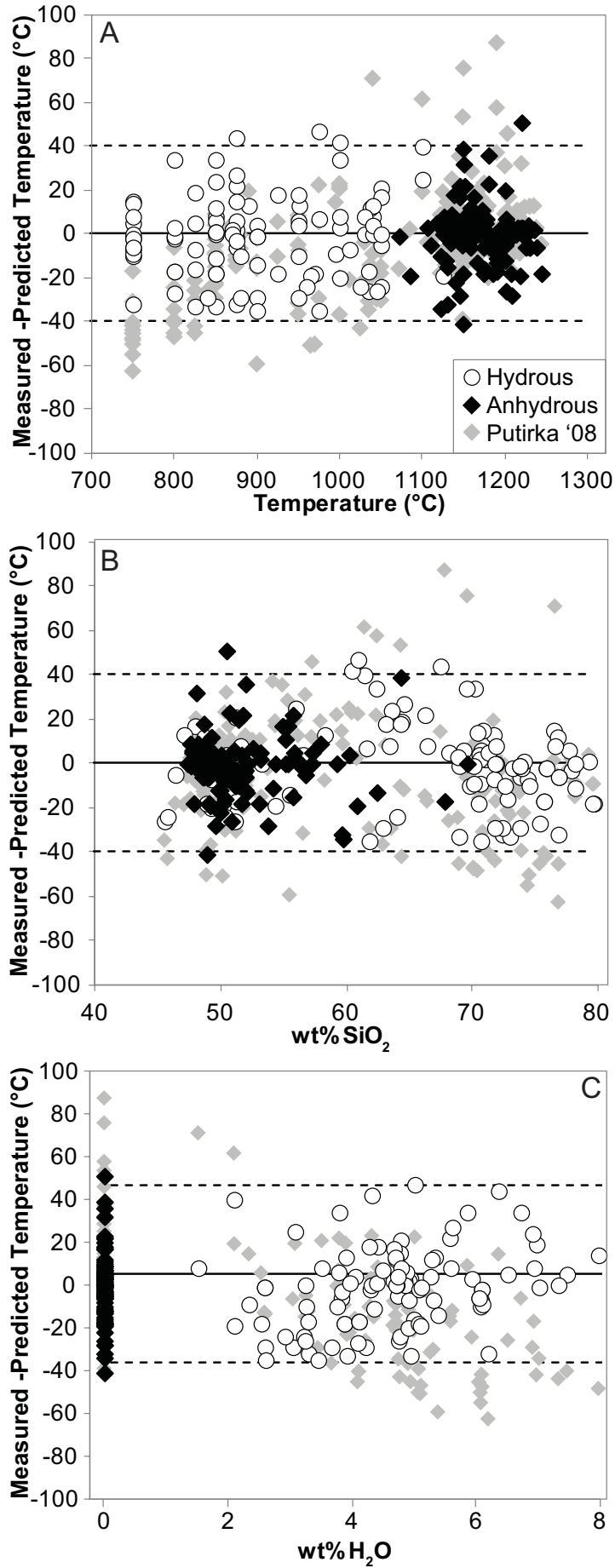


Figure 7

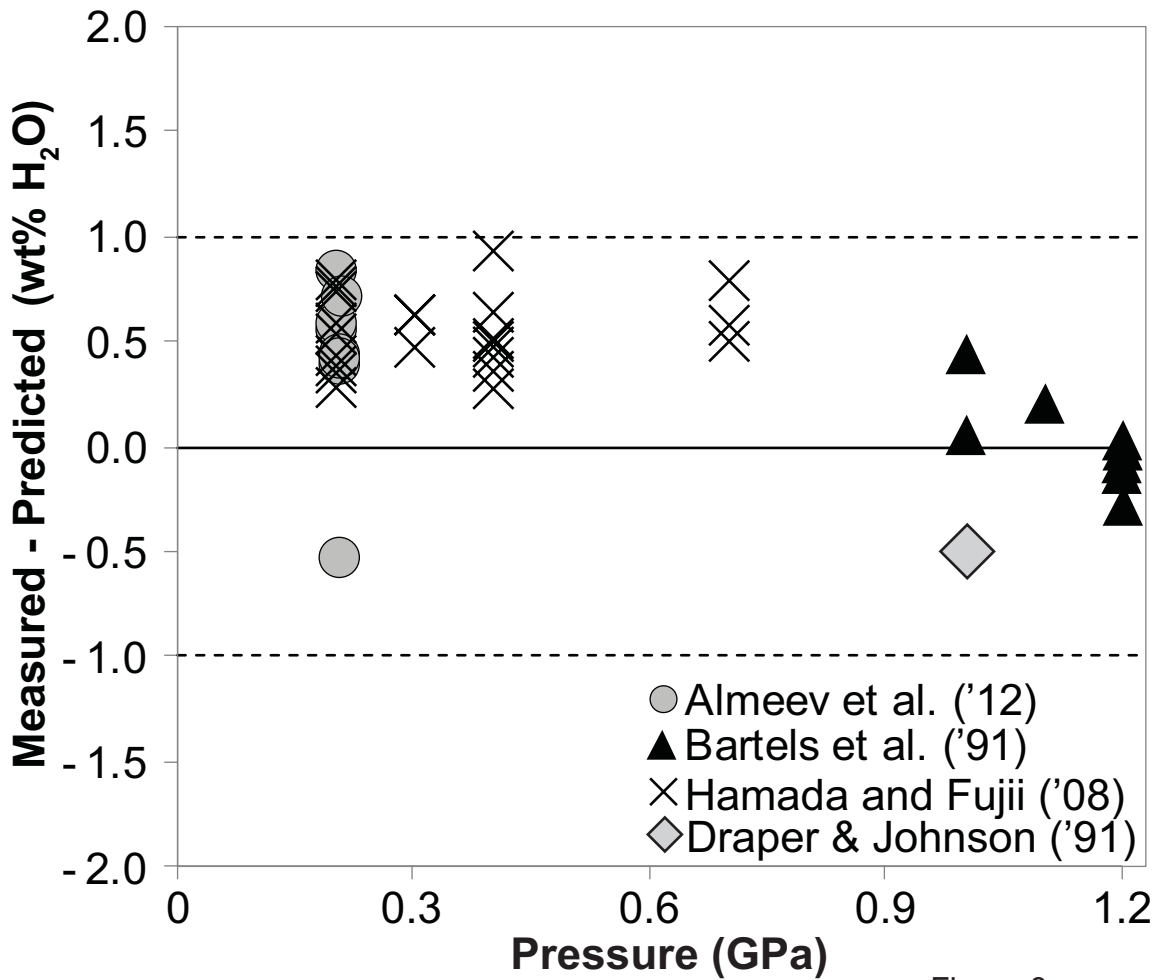


Figure 8

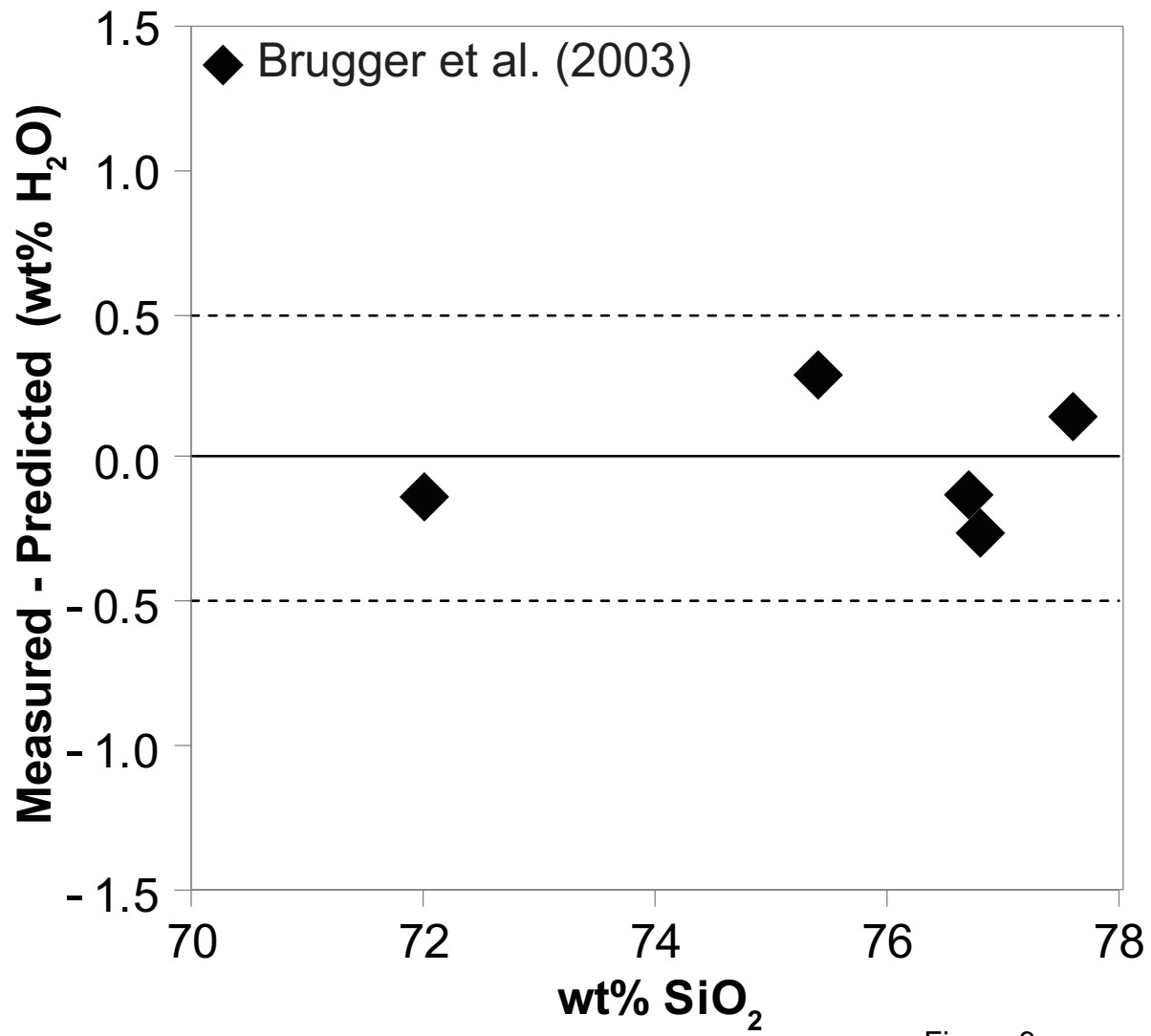


Figure 9

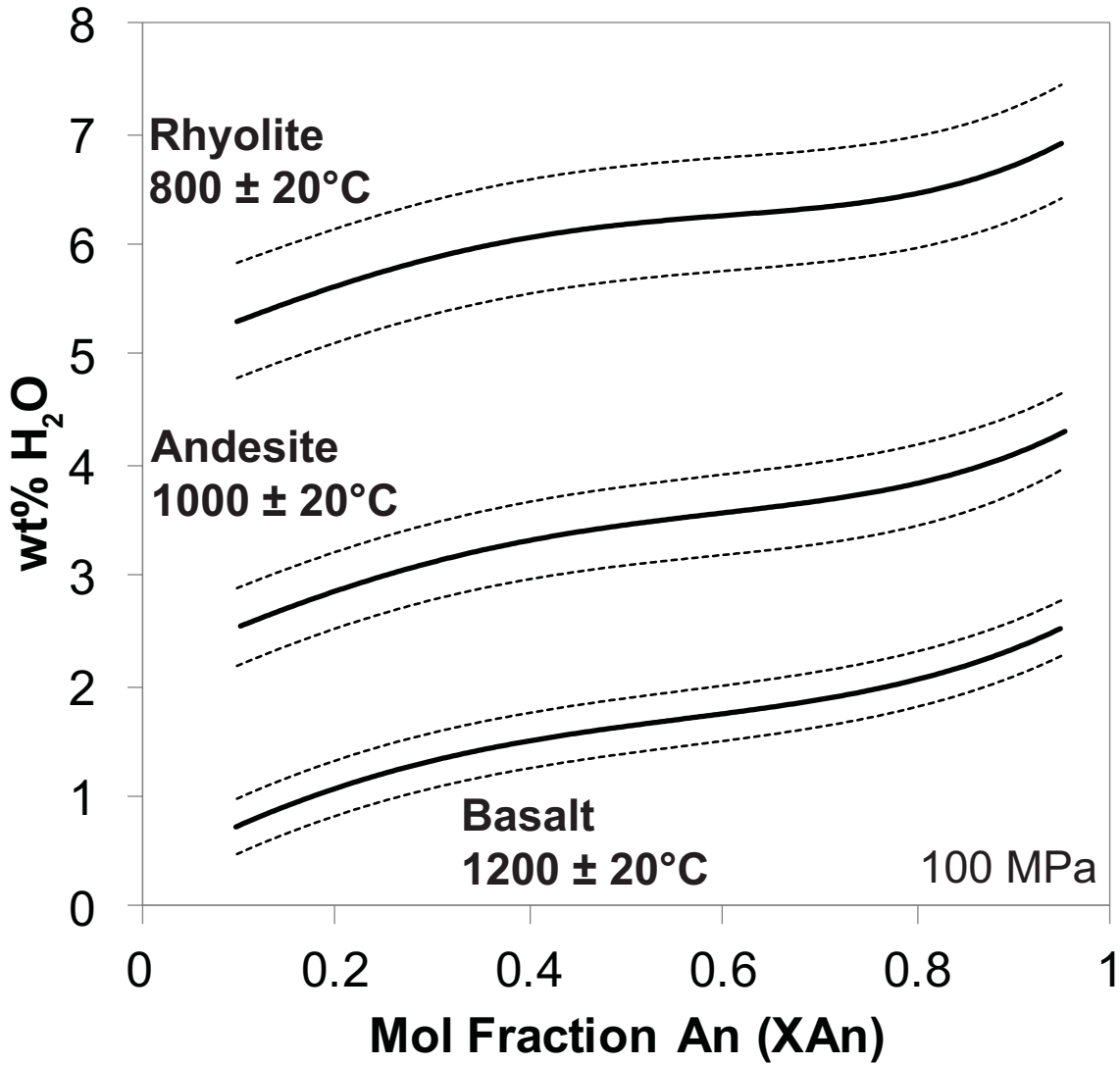


Figure 10

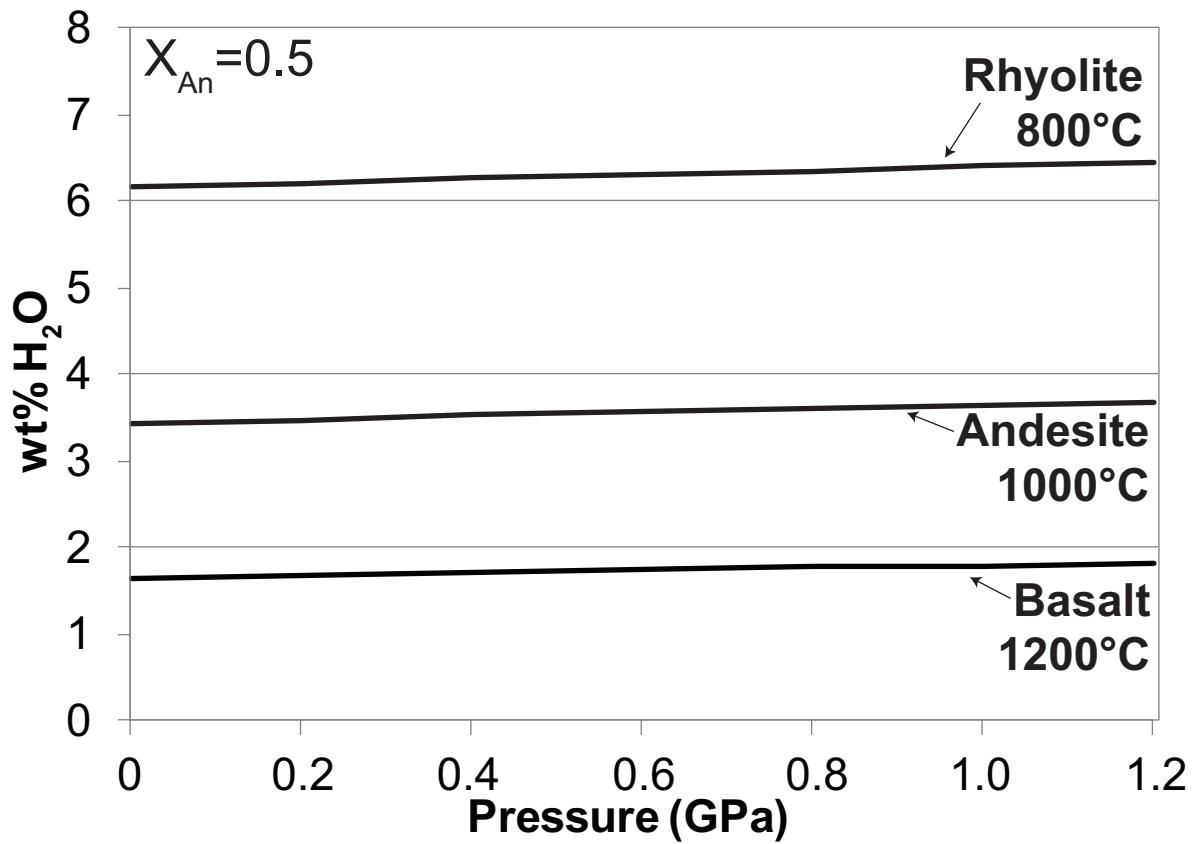


Figure 11

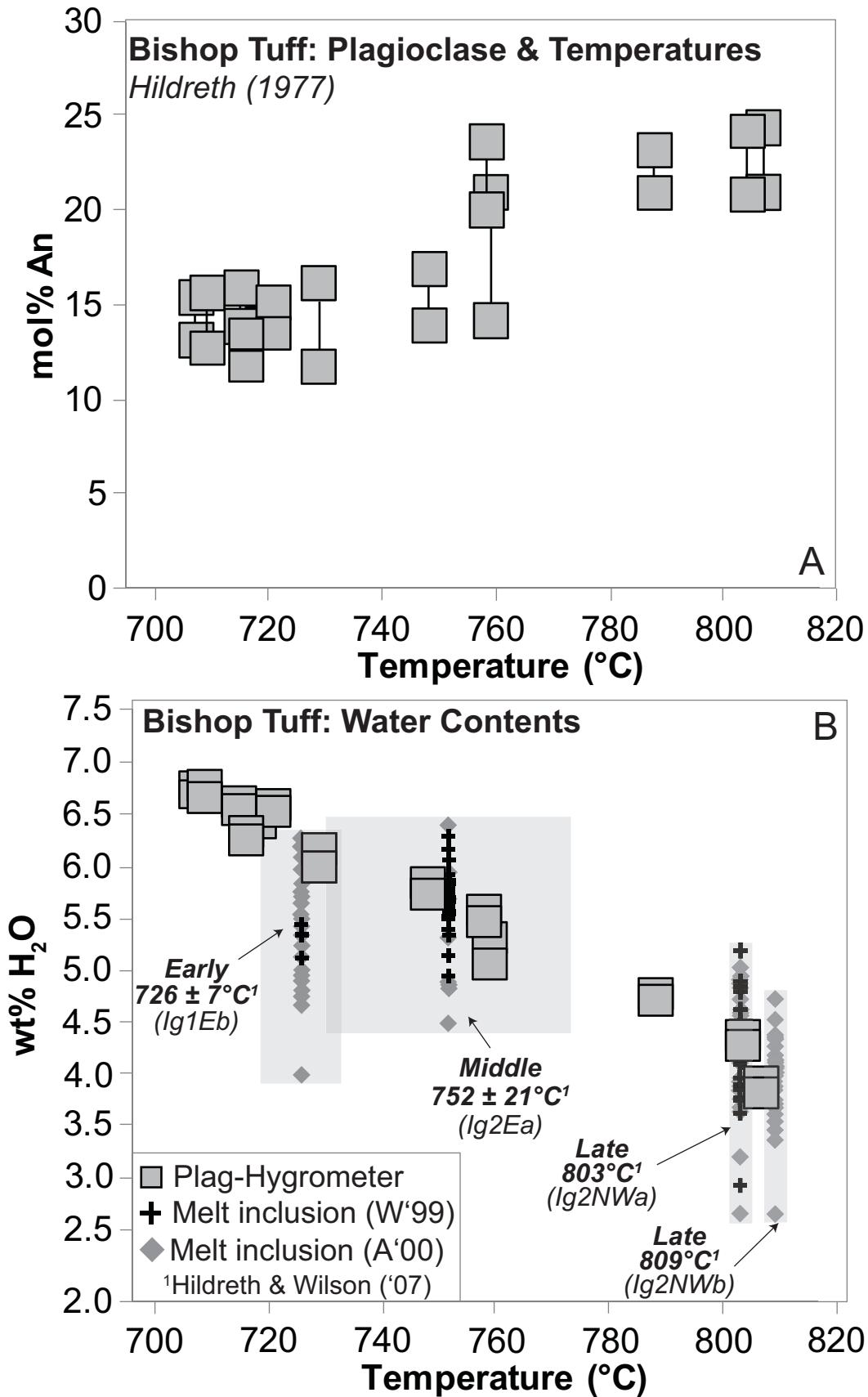


Figure 12

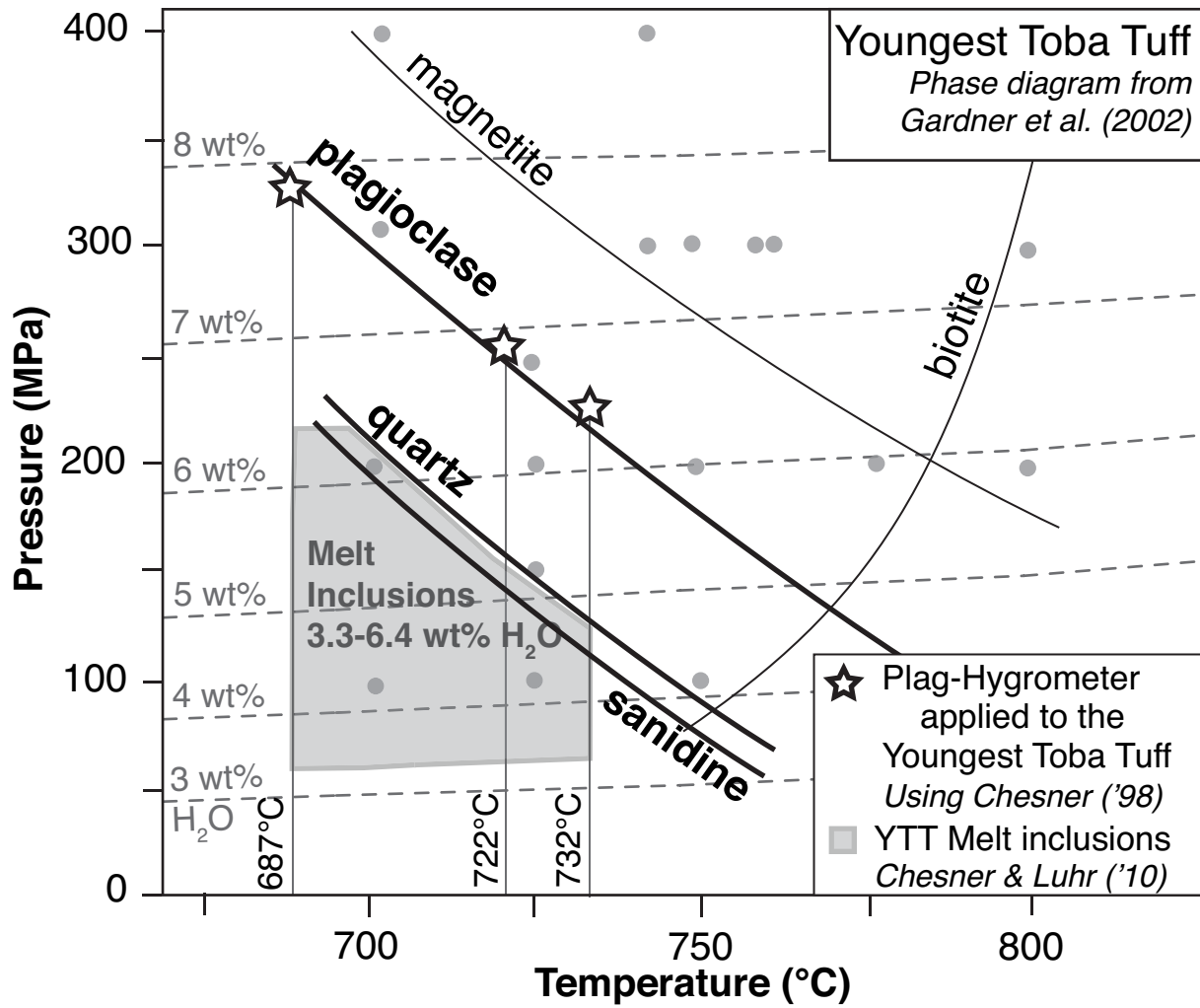


Figure 13

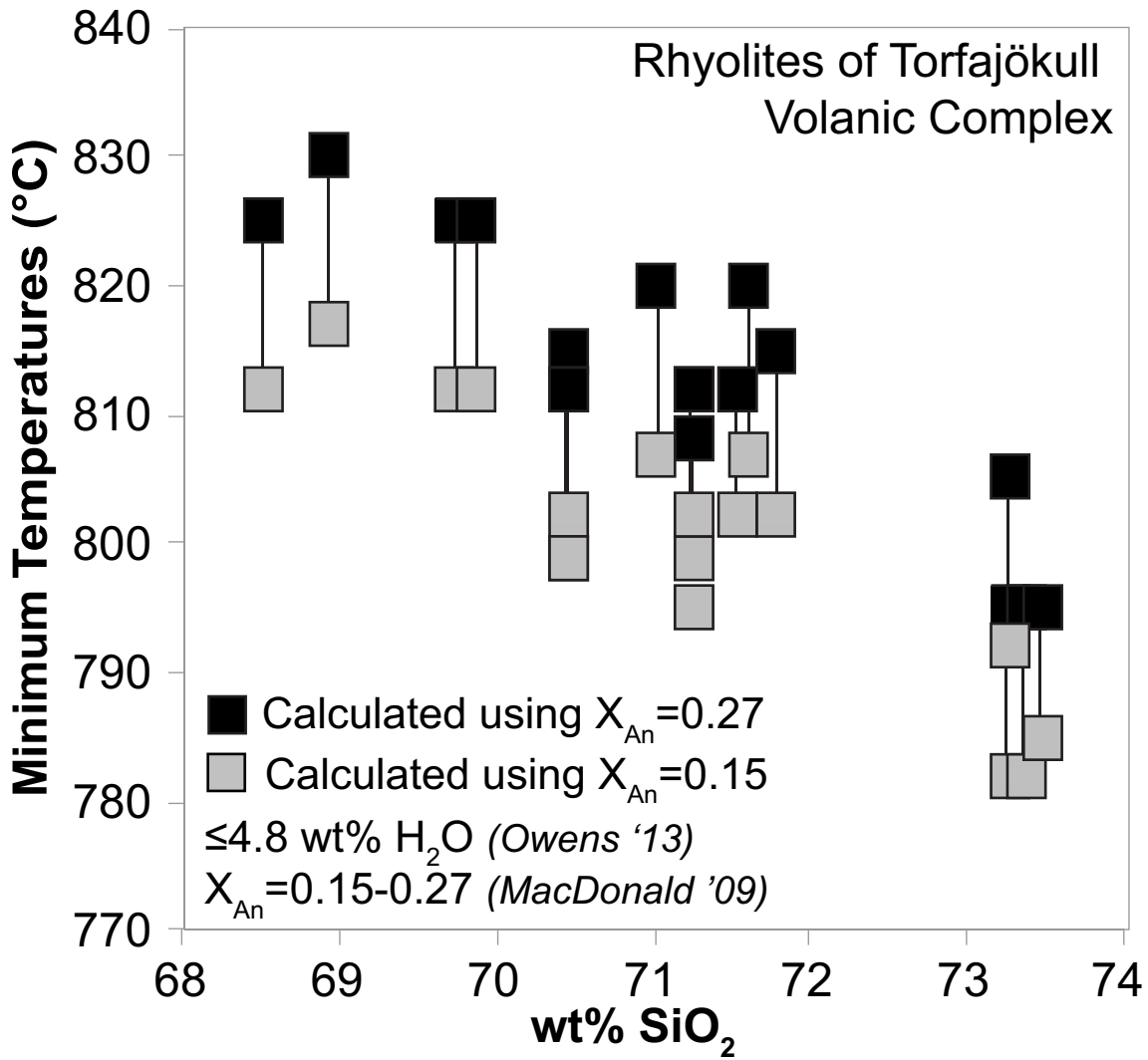


Figure 14